Mechanical Systems and Signal Processing 68-69 (2016) 587–607

Contents lists available at ScienceDirect

Mechanical Systems and Signal Processing

journal homepage: www.elsevier.com/locate/ymssp

Time-domain damping models in structural acoustics using digital filtering

Augustin Parret-Fréaud [1,*], Benjamin Cotté, Antoine Chaigne [2]

Institute of Mechanical Sciences and Industrial Applications, ENSTA ParisTech, CNRS, CEA, EDF, Université Paris-Saclay, 828 bd des Maréchaux, 91762 Palaiseau cedex, France.

ARTICLE INFO

Article history:
Received 13 November 2014
Received in revised form
27 June 2015
Accepted 4 August 2015
Available online 28 August 2015

Keywords:
Damping
Time-domain modeling
Vibroacoustics
Digital filtering

ABSTRACT

This paper describes a new approach in order to formulate well-posed time-domain damping models able to represent various frequency domain profiles of damping properties. The novelty of this approach is to represent the behavior law of a given material directly in a discrete-time framework as a digital filter, which is synthesized for each material from a discrete set of frequency-domain data such as complex modulus through an optimization process. A key point is the addition of specific constraints to this process in order to guarantee stability, causality and verification of thermodynamics second law when transposing the resulting discrete-time behavior law into the time domain. Thus, this method offers a framework which is particularly suitable for time-domain simulations in structural dynamics and acoustics for a wide range of materials (polymers, wood, foam, etc.), allowing to control and even reduce the distortion effects induced by time-discretization schemes on the frequency response of continuous-time behavior laws.

1. Introduction

Damping plays a major role in vibration of structures because of its huge influence on various characteristics of dynamical response and radiated acoustic field [1,2]. A good understanding of this phenomenon is of importance to achieve multiple goals ranging from the attenuation of noise and vibrations [3] to the improvement of efficiency regarding radiated sound fields, *e.g.* in audio transducers or musical instruments. In this context, the study and prediction of transient vibroacoustic response generated by structures under impulse-type excitation is a major field of interest which requires a fine description of damping. One may find various applications in transportation acoustics, *e.g.* in railways industry when studying impact noise generated by wheel–rail contact [4] or in building and room acoustics through the concept of auralization [5]. Another major area of application is related to the concept of sound synthesis by means of physical modeling [6] and its applications in the acoustics of musical instruments [7–9], where psychoacoustical studies have highlighted the major role played by damping on the perception of sounds [10].

For a given material, damping is often characterized in the frequency domain from experimental measurement of the complex modulus E^* or loss factor η, that may be obtained using various techniques including viscoanalyzers. Such results

* Corresponding author.
E-mail addresses: augustin.parret-freaud@safran.fr (A. Parret-Fréaud), benjamin.cotte@ensta-paristech.fr (B. Cotté), chaigne@mdw.ac.at (A. Chaigne).
[1] Present address: Safran Tech, 1 rue Geneviève Aubé, 78772 Magny les Hameaux, France.
[2] Present address: Institut für Wiener Klangstil, University of Music and Performing Arts Vienna (MDW), Anton-von-Webern Platz 1, 1030 Vienna, Austria.
URL: http://www.imsia.cnrs.fr

http://dx.doi.org/10.1016/j.ymssp.2015.08.005
0888-3270/

generally exhibit frequency behaviors which differ a lot depending on the type of observed material and on external conditions like temperature and hygrometry (see *e.g.* some experimental results for a wide range of damping materials in [11]). This leads to a wide range of frequency-domain damping models (see *e.g.* [12]), which may not be directly transferable to the time domain.

On the other hand, time-domain formalism appears to be more natural when dealing with structures excited by impulses as it naturally takes transient aspects of simulated response into account, or in presence of nonlinear vibrations. In this framework, the literature is plentiful of models initially developed in the framework of linear viscoelasticity [13]. The most simple ones are well-known Maxwell, Kelvin–Voigt and Zener (also called standard linear solid) models, whereas more sophisticated ones have been also developed, such as Golla–Huges–McTavish [14,15], anelastic displacement fields [16] or generalized Zener model, which is probably the most widely used in linear viscoelasticity [17,18]. The common basis of all those models is to describe damping behavior by combining rheological elements, such as springs, dash-pots and masses, which are expressed in the time domain by combination of time derivatives. However, their ability to approach arbitrary frequency-domain variations of a given behavior may be limited and they may require, for special shapes, a large number of coefficients. Another class of model that has been widely studied for about 20 years lies on the concept of fractional time derivatives [19]. Their main advantage lies in the ability to represent almost constant behavior in the frequency domain using only a small set of coefficients, together with being well-posed, especially concerning causality and thermodynamics aspects [20]. However, an important drawback of such types of models remains in the difficulty to transpose it into a numerical time-integration scheme in an efficient way [21], and current implementations often requires a significant number of internal variables.

Hence, providing time-domain models able to accurately describe various frequency shapes of damping properties while being in accordance with essential properties of causality, stability and positivity of dissipation remains a sensitive issue that has been recently addressed, for linear viscoelasticity, in an original way using existing mathematical works on complex analysis [22]. Moreover, in the context of numerical simulation, time-discretization schemes applied to a given continuous time-domain model have to be chosen accordingly since they often lead to distortion of its response in the frequency domain, especially in the frequency range close to the Nyquist frequency $f_s/2$ which is the maximum valid frequency associated to a sampling rate f_s according to Shannon theorem. Furthermore, it is desirable to make sure that the whole numerical scheme resulting from space-time discretization of the initial problem fulfills some discrete-time energetic identity, especially in order to guarantee the stability of the resolution [6].

The work presented here lies in the three axes mentioned above as our goal is to provide time-domain models able to depict various types of frequency dependency for damping properties, so as to be usable in the context of time-domain simulation of structures made from a wide range of materials (including wood, polymers and composites) under impulse loading. In order to take the influence of the discretization step into account, the key point of the approach described in the present paper is to directly work inside a discrete-time framework by considering the behavior law as a digital filter [23]. Given a sampling frequency corresponding to the time step of the simulation, the filter is then synthesized in the frequency domain from experimental results on complex modulus through an optimization problem involving the discrete transfer function of the filter. Essential properties as stability, causality and positivity of dissipation are ensured during the optimization process through the addition of specific constraints acting on filter coefficients. Once synthesized, the resulting filter, which corresponds to an already discretized behavior law, may be directly transposed in the discrete-time domain keeping its well-posedness. Finally, one obtains a recursive relation between values at current and previous time steps, which may be directly implemented in a discrete integration scheme, providing discrete-time energetic identity of the whole scheme as well.

This paper is organized as follows. On the basis of a one-dimensional problem that will remain the application framework throughout the paper, Section 2 introduces the formulation of discrete well-posed time-domain behavior law by means of digital filtering. Section 3 shows the constrained optimization process used to synthesize filters from experimental frequency-domain data. Section 4 describes the space-time numerical scheme to simulate structures equipped with previous models, followed by stability analysis by means of an energetic approach and study of errors induced by numerical dispersion and dissipation. Section 5 presents numerical assessments that (1) describes the whole process of modeling and time-domain simulation of a structure given experimental frequency-domain results and (2) validate the whole approach, especially regarding numerical errors.

2. Time domain modeling by means of digital filtering

2.1. Model problem

The present development, mainly those regarding the integration scheme, is realized in the context of one-dimensional mechanical problems. To present the method in a simple context, we consider below the longitudinal vibrations of a cantilever beam under the classical small perturbations hypothesis (Fig. 1).

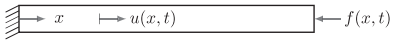

Fig. 1. Cantilever beam schematics.

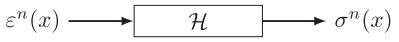

Fig. 2. Digital filter $\mathcal{H}$ representing the continuous constitutive law $\mathcal{E}$.

Denoting $u(x,t)$, $\varepsilon(x,t)$ and $\sigma(x,t)$ the displacement, strain and stress fields, respectively, and applying Newton second law, leads to the following system of equations:

$$\sigma(x,t)=\mathcal{E}(\varepsilon(x,t))=\mathcal{E}\left(\frac{\partial u(x,t)}{\partial x}\right), \tag{1a}$$

$$\rho(x)\frac{\partial^2 u(x,t)}{\partial t^2}=\frac{\partial \sigma(x,t)}{\partial x}+f(x,t), \tag{1b}$$

where the constitutive law $\mathcal{E}$ is assumed to be local, linear and time-invariant, $\rho(x)$ denotes the volumetric mass density and $f(x,t)$ an external volumetric force density. We also consider the following boundary conditions: $u(x,0)=0$ and $\sigma(x,L)=0$. In the following (Section 5), let us note that $f(x,t)$ will be chosen as $f(x,t)=F(t)\delta(x-L)$, with $F(t)$ a given time function and δ denoting the dirac distribution, in order to model an impact on the right end of the beam.

2.2. Discrete-time constitutive relation by digital filtering

Instead of discretizing a continuous time-domain model, we decide to represent it directly in the discrete-time space by a digital filter $\mathcal{H}$ (Fig. 2). In order to achieve this, we first introduce a time discretization step Δt corresponding to a sampling frequency $f_s=\Delta t^{-1}$ and we denote $\sigma^n(x)=\sigma(x,t^n)$ and $\varepsilon^n(x)=\varepsilon(x,t^n)$ the values of stress and strain field at time $t^n=n\Delta t$.

In accordance with the hypothesis of linearity and time-invariance on $\mathcal{E}$, one can express the filter $\mathcal{H}$ in the time domain as a linear recursive relation involving values of σ and ε at current and previous time steps [23]:

$$\sigma^{n+1}(x)=\mathcal{H}\left(\sigma^n(x),\ldots,\sigma^{n+1-N_d}(x),\varepsilon^{n+1}(x),\ldots,\varepsilon^{n+1-N_c}(x)\right)=H_0\left(\varepsilon^{n+1}(x)+\sum_{l=1}^{N_c}c_l\varepsilon^{n+1-l}(x)\right)-\sum_{m=1}^{N_d}d_m\sigma^{n+1-m}(x). \tag{2}$$

where H_0, $\{c_l\}_l$ and $\{d_m\}_m$ denote time-invariant coefficients.

The Z-transform (denoted TZ) provides a convenient way to synthetize the filter $\mathcal{H}$ and study its properties in the frequency domain. Given a sequence of discrete samples $\{v^n\}_n$ at different time t^n, the corresponding Z-transform $\check{v}(z)$ is given by

$$\text{TZ: }\{v^n\}_n\longmapsto\check{v}(z)=\sum_{n=-\infty}^{\infty}v^n z^{-n}. \tag{3}$$

Applying TZ to the discrete-time constitutive relation (2) gives the complex Z-transfer function $H(z)$ as

$$H(z)=\frac{\check{\sigma}(x,z)}{\check{\varepsilon}(x,z)}=H_0\left[\frac{1+\sum_{l=1}^{N_c}c_l z^{-l}}{1+\sum_{m=1}^{N_d}d_m z^{-m}}\right], \tag{4}$$

where $\check{\sigma}(x,z)$ (resp. $\check{\varepsilon}(x,z)$) is the Z-transform of $\{\sigma^n(x)\}_n$ (resp. $\{\varepsilon^n(x)\}_n$). The transfer function H may be equally written in a form involving its poles $(p_m)_{1\le m\le N_d}$ and zeros $(q_l)_{1\le l\le N_c}$ as

$$H(z)=H_0\left[\frac{\prod_{l=1}^{N_c}(1-q_l z^{-l})}{\prod_{m=1}^{N_d}(1-p_m z^{-m})}\right]. \tag{5}$$

Let us note that this last expression is particularly interesting as many properties of digital filters derive from conditions on the poles and zeros of their transfer functions. Within the scope of the present study, the very first properties to fulfill are the stability and causality of the digital filter $\mathcal{H}$. Those properties are satisfied by the necessary and sufficient condition on the poles $(p_m)_{1\le m\le N_d}$ of the transfer function which have to remain strictly inside the unit circle (see *e.g.* [24]):

$$|p_m|<1,\quad 1\le m\le N_d. \tag{6}$$

In the following, this last condition will be the first mandatory constraint imposed to any synthesis process of $\mathcal{H}$.

For the rest of the paper, instead of working with the general expression (5), we restrict ourselves to the class of transfer functions H resulting from the sum of N_f one-pole sub-filter H_k together with a constant function (pure gain) H_0:

$$H(z)=H_0+\sum_{k=1}^{N_f}H_k(z)=H_0+\sum_{k=1}^{N_f}\frac{H_{0k}}{1-p_k z^{-1}}. \tag{7}$$

The previous expression is actually the partial fraction expansion of every transfer function (5) satisfying $N_c=N_d=N_f$ and having poles of unit multiplicity, which restricts our scope to the discrete models which exclude elementary filters with multiple or complex conjugate poles. This fundamental assumption has been done to simplify the energy-based stability analysis performed in Section 4.2. Also, let us note that using a parallel association process with poles of unit multiplicity is a common approach in continuous-domain identification (*e.g.* generalized Zener model) which seems to perform well for a

wide class of viscoelastic materials. Besides, from a practical point of view, the optimization algorithm used in Section 3 in order to synthetize filter H from continuous frequency-domain data allows the poles of the transfer function to be as close as possible if needed.

2.3. Properties of one-pole filters H_k in the continuous frequency domain

Before going further into details about the synthesis of filter H based on experimental complex modulus, we will describe here the main properties of the continuous frequency response $H_k^c(\omega)$ (where ω denotes the angular frequency) of one-pole elementary filters $H_k(z)$ when poles p_k satisfy condition (6). Such a response is usually obtained by evaluating $H_k(z)$ on the unit circle by means of the change of variable $z \leftarrow \exp\left(i\omega f_s^{-1}\right)$:

$$H_k^c(\omega) = H_{k,r}^c(\omega) + iH_{k,i}^c(\omega) \quad (\omega \in [0, \pi f_s^{-1}]), \tag{8}$$

with

$$H_{k,r}^c(\omega) = H_{0,k}\frac{1-p_k\cos(\omega f_s^{-1})}{1+p_k^2-2p_k\cos(\omega f_s^{-1})}, \tag{9a}$$

$$H_{k,i}^c(\omega) = -H_{0,k}\frac{p_k\sin(\omega f_s^{-1})}{1+p_k^2-2p_k\cos(\omega f_s^{-1})}. \tag{9b}$$

The derivation of $H_{k,r}^c$ with respect to ω gives

$$\frac{dH_{k,r}^c}{d\omega}(\omega) = -H_{0,k}p_k\frac{(1-p_k^2)f_s^{-1}\sin(\omega f_s^{-1})}{\left(1+p_k^2-2p_k\cos(\omega f_s^{-1})\right)^2},$$

such that when hypothesis (6) on p_k is verified, $H_{k,r}^c$ is a monotonously increasing function if $H_{0,k}p_k \leq 0$, with the following extrema:

$$H_{k,r}^c\min = H_{k,r}^c(0) = \frac{H_{0,k}}{1-p_k}, \tag{10a}$$

$$H_{k,r}^c\max = H_{k,r}^c(\pi f_s) = \frac{H_{0,k}}{1+p_k}, \tag{10b}$$

$$|\Delta H_{k,r}^c| = |H_{k,r}^c\max - H_{k,r}^c\min| = \frac{2|H_{0,k}p_k|}{1-p_k^2}. \tag{10c}$$

The same applied to $H_{k,i}^c$ gives

$$\frac{dH_{k,i}^c}{d\omega}(\omega) = H_{0,k}p_k f_s^{-1}\frac{(2p_k-(1+p_k^2)\cos(\omega f_s^{-1}))}{\left(1+p_k^2-2p_k\cos(\omega f_s^{-1})\right)^2}$$

such that $H_{k,i}^c$ vanishes at $\omega = 0$ and $\omega = \pi f_s$ and admits a unique extremum $H_{k,i}^c\max$ at $\omega_{\max}^{H_{k,i}^c}$ given by

$$H_{k,i}^c\max = -\frac{H_{0,k}p_k}{1-p_k^2}, \quad \omega_{\max}^{H_{k,i}^c} = f_s\arccos\left(\frac{2p_k}{1+p_k^2}\right). \tag{11}$$

Thus, $H_{k,i}^c(\omega) \geq 0$ as soon as $H_{0,k}p_k \leq 0$ and (6) is satisfied. Finally, Fig. 3 shows the response $H_{k,r}^c$ and $H_{k,i}^c$ of filter H_k for different values of p_k satisfying (6).

2.4. Well-posedness of the complete model in the continuous frequency domain

Let us now consider the continuous frequency response $H^c(\omega)$ of the filter H given by (7), which can be written as

$$H^c(\omega) = H_r^c(\omega) + iH_i^c(\omega) \quad (\omega \in [0, \pi f_s^{-1}]), \tag{12}$$

with

$$H_r^c(\omega) = H_0 + \sum_{k=1}^{N_f} H_{0,k}\frac{1-p_k\cos(\omega f_s^{-1})}{1+p_k^2-2p_k\cos(\omega f_s^{-1})}, \tag{13a}$$

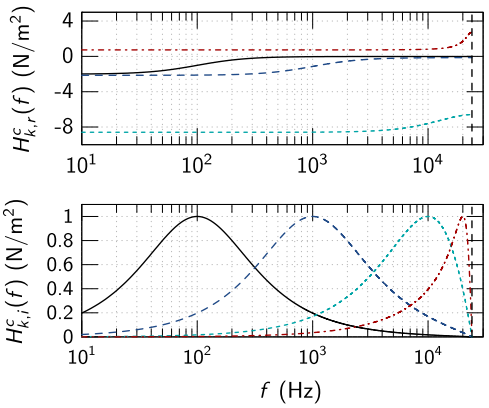

Fig. 3. $H^c_{k,r}$ and $H^c_{k,i}$ for values of p_k satisfying (6) and $H_{0k}p_k \leq 0$ ($f_s = 48$ kHz): p_k=0.99 (—), p_k=0.88 (– –), p_k=0.13 (- -) and $p_k = -0.58$ (– ·). The vertical dashed line corresponds to $f_s/2$.

$$H^c_i(\omega) = -\sum_{k=1}^{N_f} H_{0,k}\frac{p_k \sin(\omega f_s^{-1})}{1+p_k^2-2p_k\cos(\omega f_s^{-1})}. \tag{13b}$$

Taking the continuous frequency-domain transposition of Eq. (4), one has

$$H^c(\omega) = \frac{\hat{\sigma}(x,\omega)}{\hat{\varepsilon}(x,\omega)}, \tag{14}$$

where $\hat{v}(x,\omega)$ stands for the partial time Fourier transform of $v(x,t)$ given for causal signals by

$$\hat{v}(x,\omega) = \int_0^\infty v(x,t)\exp(-i\omega t)\,dt. \tag{15}$$

From a mechanical point of view, Eq. (14) defines the usual complex modulus of a given material as the ratio of the Fourier transform of stress and strain. Thus, we may interpret $H^c(\omega)$ as the complex modulus in the continuous frequency-domain associated with a discrete-time behavior law defined by filter H. In order to obtain a well-posed model, the first additional condition to impose is the positivity of the static modulus as

$$H^c(0) = H(1) \geq 0. \tag{16}$$

Furthermore, the global loss factor η^H and elementary ones η^H_k associated to elementary one-pole filters may be introduced in a similar way as for the complex modulus:

$$H^c(\omega) = H^c_r(\omega)(1+i\eta^H(\omega)) = H^c_r(\omega)\left(1+i\sum_{k=1}^{N_f}\eta^H_k(\omega)\right), \quad \text{with } \eta^H_k(\omega) = \frac{H^c_{k,i}(\omega)}{H^c_r(\omega)}. \tag{17}$$

In order to obtain a dissipative model in accordance with the second law of thermodynamics, we choose to impose the positivity of each loss factor η^H_k, so as to ensure each internal process act as a dissipative one. From Eqs. (9b) and (13a), this may be enforced by the following condition acting on the coefficients of H_k:

$$H_{0,k}p_k \leq 0, \quad \forall k, \tag{18}$$

which ensure functions $H^c_{i,k}$ to be positive and $H^c_{r,k}$ to be monotonously increasing, as already seen in Section 2.3. This last property, together with condition (16) on poles p_k, ensure positivity of H^c_r, and thus of each function η^H_k on the whole frequency range. Let us note that condition (18) is only a sufficient one to obtain a positive global loss factor η^H and the dissipation property of the underlying behavior. Indeed, we may exhibit filters constituted of some components with negative dissipation, which may be balanced by the overall dissipation induced by the remaining ones so that the global loss factor η^H remains positive on the whole frequency range. As one must be careful when dismissing a model which is itself physical only because some of its elementary components appear to be not physical, it would be probably interesting to try to relax this constraint in future works even if it might complicate the whole synthesis process.

3. Synthesis of filter $\mathcal{H}$ from frequency-domain damping data

Given a set $\{E^*_j\}_j$ of values of Young's modulus at various frequencies $\{\omega_j\}_j$, which may be results of experimental procedures, this section is devoted to the description of the optimization process that allows us to synthesize the filter $H(z)$ previously introduced. The underlying problem consists in finding parameters $H_0, \{H_{0,k}, p_k\}_k$ minimizing the distance

between the continuous response $H^c(\omega)$ of filter $\mathcal{H}$ and the value E_j^* at each frequency ω_j, while ensuring conditions (6), (16) and (18) in order to guarantee the well-posedness of the corresponding discrete-time model. From a general point of view, finding an efficient method to correctly identify a material law from data given in the complex plane is still a tricky task, though it has been recently addressed in some original way when identifying rheological behaviors, using mathematical results from complex analysis [22] or graphical methods stemming from the field of system automation [25].

3.1. Cost function and constrained optimization problem

In the following, we choose to work with a non-linear least-square problem by directly measuring the distance between H^c and the input data using the classical quadratic norm on both real and imaginary part. Denoting $X=\left[H_0,\{H_{0,k},p_k\}_k\right]^T$ the vector containing filter parameters, the resulting cost function $\mathcal{L}$ to be minimized is

$$\mathcal{L}(X)=\alpha_r\mathcal{L}_r(X)+\alpha_i\mathcal{L}_i(X),\ =\alpha_r\left[\sum_j\left(\frac{H_r^c(\omega_j)-\mathcal{R}e\left(E_j^*\right)}{\mathcal{R}e\left(E_j^*\right)}\right)^2\right]^{1/2}\quad+\alpha_i\left[\sum_j\left(\frac{H_i^c(\omega_j)-\mathcal{I}m\left(E_j^*\right)}{\mathcal{I}m\left(E_j^*\right)}\right)^2\right]^{1/2},\tag{19}$$

where α_r and α_i are scaling coefficients, which will be set to 1 in the following.

In order to study the sensitivity of the cost function $\mathcal{L}$ to the parameters of the optimization process, we first express, for an arbitrary parameter Z, the partial derivative of $\mathcal{L}$ with respect to Z as a function involving the sensitivity of H^c:

$$\partial_Z\mathcal{L}=\alpha_r\mathcal{L}_r^{-1}\sum_j\left(\frac{H_r^c(\omega_j)-\mathcal{R}e\left(E_j^*\right)}{\mathcal{R}e\left(E_j^*\right)^2}\partial_Z H_r^c(\omega_j)\right)\quad+\alpha_i\mathcal{L}_i^{-1}\sum_j\left(\frac{H_i^c(\omega_j)-\mathcal{I}m\left(E_j^*\right)}{\mathcal{I}m\left(E_j^*\right)^2}\partial_Z H_i^c(\omega_j)\right)$$

Then, the derivative of H_r^c and H_i^c with respect to H_0, $H_{0,k}$ and p_k may be written from (7), (9a) and (9b) as

$$\begin{aligned}
&\partial_{H_0}H_r^c(\omega)=1,\\
&\partial_{H_0}H_i^c(\omega)=0,\\
&\partial_{H_{0,k}}H_r^c(\omega)=\frac{1-p_k\cos(\omega f_s^{-1})}{1+p_k^2-2p_k\cos(\omega f_s^{-1})},\\
&\partial_{H_{0,k}}H_i^c(\omega)=-\frac{p_k\sin(\omega f_s^{-1})}{1+p_k^2-2p_k\cos(\omega f_s^{-1})},\\
&\partial_{p_k}H_r^c(\omega)=H_{0,k}\frac{(1+p_k^2)\cos(\omega f_s^{-1})-2p_k}{\left(1+p_k^2-2p_k\cos(\omega f_s^{-1})\right)^2},\\
&\partial_{p_k}H_i^c(\omega)=-H_{0,k}\frac{(1-p_k^2)\sin(\omega f_s^{-1})}{\left(1+p_k^2-2p_k\cos(\omega f_s^{-1})\right)^2}.
\end{aligned}$$

Previous equations show that the sensitivity of $\mathcal{L}$ to coefficients p_k, which follows directly from those of $\partial_{p_k}H_r^c$ and $\partial_{p_k}H_i^c$, is scaled by $H_{0,k}$, which is not the case concerning the sensitivity with respect to H_0 and $H_{0,k}$. Unfortunately, this may lead to a huge lack of sensitivity to the last parameters, and thus poor performance of the minimization algorithm as $H_{0,k}$ may be several order of magnitude above those of p_k (typically 10^9 versus 0.1). To overcome this issue, we apply some partial scaling to the filter parameters by scaling coefficients H_0 and $H_{0,k}$ with a reference value $\tilde{H}$ (typically $\tilde{H}=\max_j\left(\left|E_j^*\right|\right)$) prior to the optimization process.

Finally, the constrained optimization problem to be solved writes in a generic way as

$$\begin{aligned}
&\text{find } \tilde{X}=\left[\tilde{H}_0,\left\{\tilde{H}_{0,k},p_k\right\}_k\right]^T\quad\text{verifying } \min_{\tilde{X}}\mathcal{L}(\tilde{X})\\
&\text{subject to constraints}\quad \mathcal{C}_i(\tilde{X})>0,
\end{aligned}\tag{20}$$

where $\tilde{H}_0=H_0/\tilde{H}$, $\tilde{H}_{0,k}=H_{0,k}/\tilde{H}$, and function $\mathcal{C}_i$ contains the constraints (6), (16) and (18) on the filter coefficients:

$$\mathcal{C}_i(\tilde{X})=\begin{bmatrix}1-|p_1|\\ \vdots\\ 1-|p_{N_f}|\\ \tilde{H}^c(0)\\ -\tilde{H}_{0,1}p_1\\ \vdots\\ -\tilde{H}_{0,N_f}p_{N_f}\end{bmatrix}.\tag{21}$$

From the previous choices, we get a general non-linear optimization problem on both the cost function and the inequality constraints, which is unfortunately non-convex and exhibits several local minima. In order to solve it, we use a general-purpose algorithm devoted to non-linear optimization problems, namely the classical sequential quadratic programming algorithm [26] and its implementation in the GNU/Octave programming language (provided by `sqp` function). In practice, this algorithm, which is in some ways close to Newton's method, solves in an iterative way a set of sub-problems defined by both quadratic approximation of the cost function and linear approximation of the constraints.

So far, let us note that the setup of a more optimal cost function, which may *e.g.* make the overall optimization problem more robust or take into account some external factors like noisy data, is still an open problem and will be studied in future works.

3.2. Application to a visco-elastic material

We now apply the previous described approach to complex modulus data related to polyurethane 24-8-1 foam at 20 °C, taken from AFWAL-TR-84-3089 technical report [11], the sampling frequency f_s being set to 80 kHz. In order to illustrate the synthesis process, we repeat it in an iterative way to build a set of filters defined by Eq. (7) with an increasing number N_f of one-pole sub-filters, until we obtain a satisfactory frequency representation of the input data. First, we introduce the frequency range of interest $[f_{\min},f_{\max}]$ on which we want to synthesize the filter and we divide it into N_f logarithmically spaced intervals $[f_k,f_{k+1}]$ $(0\leq k\leq N_f-1)$, with $f_0=f_{\min}$, $f_{N_f}=f_{\max}$, $f_k=f_{\min}(\Delta f)^k$ $(1\leq k\leq N_f-1)$ and $\Delta f=(f_{\max}/f_{\min})^{1/N_f}$. Then, prior to the optimization process, we initialize the pole p_k of every sub-filter H_k in order to have the imaginary part of its response reaching its maximum $H^c_{k,i}\max$, as given by Eq. (11), on the logarithmic center frequency $f_{k+1/2}=\sqrt{f_k f_{k+1}}$ of each interval $[f_k,f_{k+1}]$.

In the following, the values of $[f_{\min},f_{\max}]$ have been set to [10 Hz, 25 kHz], which covers the frequency range of the experimental data available from the report. As we are mostly interested in the frequencies in the audible range, which is approximately [20 Hz, 20 kHz], the critical material behavior below 10 Hz will not have a strong impact on our predictions. For a given iteration p corresponding to the synthesis of a filter with $N_f=p$ one-pole sub-filters, we denote $\mathcal{L}(X_p)$ the associated error coming from the optimization process, that is the cost function (19) applied on the set X_p containing the parameters of the resulting filter. Recall that $\mathcal{L}(X_p)$ measures the gap between the response of the synthesized filter and the input data. In order to assess the convergence of the whole iterative procedure previously described, we also introduce the relative error $e_{\mathcal{L},p}$ measuring the variation of $\mathcal{L}(X_p)$ between two successive iterations, as

$$e_{\mathcal{L},p}=\frac{|\mathcal{L}(X_{p-1})-\mathcal{L}(X_p)|}{|\mathcal{L}(X_{p-1})|}\quad(2\leq p\leq N_f). \tag{22}$$

Fig. 4 shows the complex modulus data and the continuous frequency-domain response of synthesized filters starting from $N_f=1$ sub-filters until the iterative procedure has converged.

While the representation of discrete data by a filter with only 1 or 2 one-pole sub-filters (see Fig. 4(a) and (b)) gives a far too coarse description, especially concerning the imaginary part of the complex modulus which is so crucial for an accurate description of damping, we notice that the model begins to be accurate from 3 sub-filters (Fig. 4(c)). As shown by Fig. 4(e), a digital filter with 5 sub-filters (whose coefficients are detailed in Table 1) seems to be the best approximation achievable regarding the relative dispersion of input data. Indeed, requesting another sub-filter in the model leads to exactly the same behavior as the one given by 5 sub-filters, as shown by Fig. 4(f).

On this particular example, let us note a crucial behavior regarding the frequency response of discrete-time models, whose imaginary part H^c_i vanishes at Nyquist frequency. Consequently, the closer the upper limit of the frequency range of interest $f_{\max}$ to Nyquist frequency $f_s/2$ is, the sharper H^c_i should be between $f_{\max}$ and $f_s/2$ in order to accurately describe behavior until $f_{\max}$. Thus, it requires to use one or more sub-filters with maxima close to $f_{\max}$ in order to get a sharp behavior, as can be seen from Fig. 4(c) to (e). Another solution would be to increase sampling frequency in order to move Nyquist frequency further away from the upper limit of the frequency range of interest, thus allowing to represent the transition between $f_{\max}$ and $f_s/2$ with smoother sub-filters. Unfortunately, it may also result in a significant increase of the computational load of the numerical simulation that follow, as it corresponds to a reduction of the time step. Consequently, as a general rule, we should keep f_s as small as possible to save computational costs while ensuring the best representation of the initial data by the synthesized filter.

Before concluding this section on filter synthesis, we must emphasize that the quality of the synthesized filter is highly dependent on the accuracy of the experimental values used as input, since we are generally dealing with noisy data to identify the filter parameters. Several research groups have proposed identification techniques that take into account input/output error noise, among which we can cite Mossberg et al. [27] and Pintelon et al. [28], who give complex modulus estimates together with their associated standard deviation or uncertainty bound. Another approach is followed by Collet et al. [22], who propose a noise-correction method of complex Young modulus measurements based on the three constraints of causality, positivity of the dissipation rate and reality of the relaxation function. In the future, such methods could be used to build new filter synthesis algorithms, where a confidence interval will be considered and not only exact frequency-domain data points.

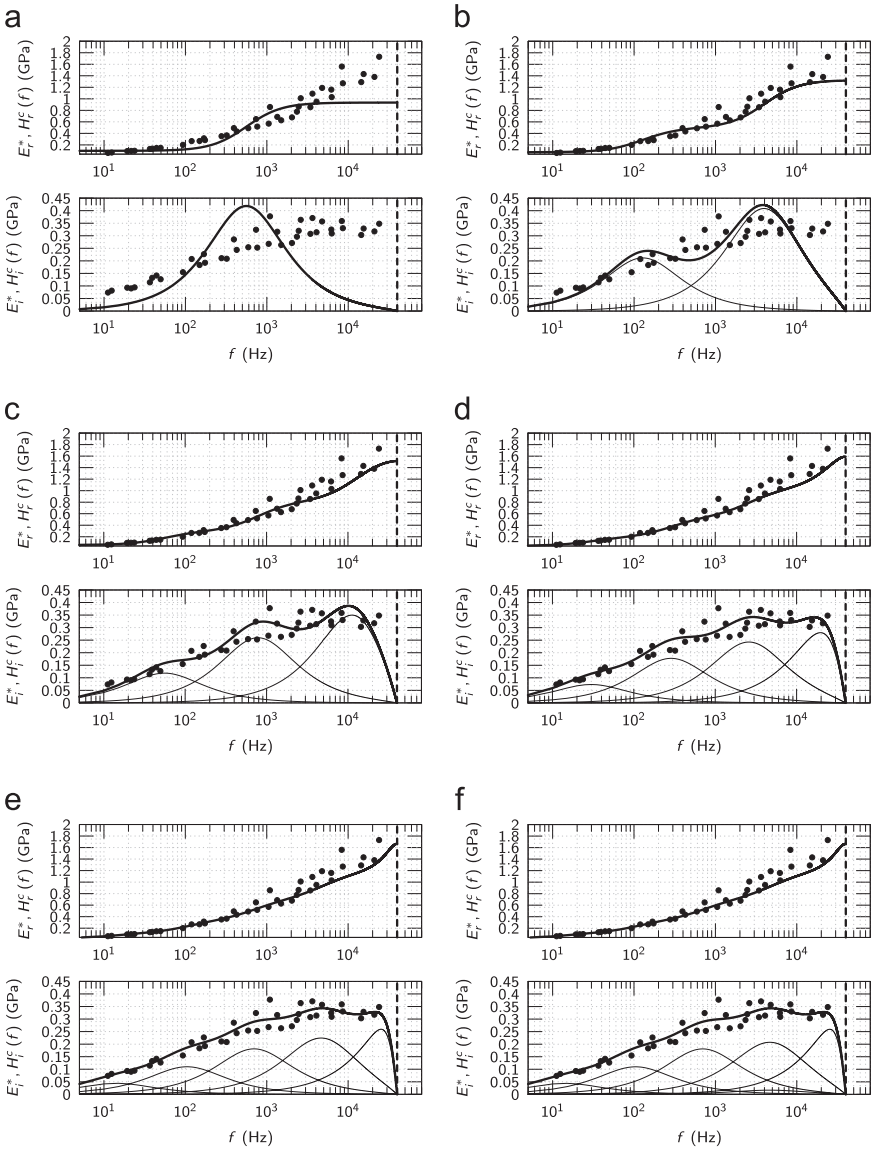

Fig. 4. Input data (solid circles) and continuous frequency-domain response (solid curves) of synthesized filter obtained with increasing number N_f of one-pole sub-filters. Thick curves show the response H^c of the whole filter whereas thin curve show the contribution H_k^c of each elementary filter to the imaginary part of the response. Nyquist frequency $f_s/2$ is represented by black dashed lines. (a) $N_f=1$, $\mathcal{L}(X_1)=5.62$. (b) $N_f=2$, $\mathcal{L}(X_2)=2.81$, $e_{\mathcal{L},2}=50.1\%$. (c) $N_f=3$, $\mathcal{L}(X_3)=1.75$, $e_{\mathcal{L},3}=37.7\%$. (d) $N_f=4$, $\mathcal{L}(X_4)=1.48$, $e_{\mathcal{L},4}=15.2\%$. (e) $N_f=5$, $\mathcal{L}(X_5)=1.36$, $e_{\mathcal{L},5}=8.1\%$. (f) $N_f=6$, $\mathcal{L}(X_6)=1.36$, $e_{\mathcal{L},6}=0\%$.

Table 1
Coefficients of synthesized filter $\mathcal{H}$ related to polyurethane 24-8-1 for $N_f=5$.

$H_0, H_{0,k}$	p_k
$9.8987 \cdot 10^8$	
$-9.8006 \cdot 10^4$	$9.9889 \cdot 10^{-1}$
$-1.8068 \cdot 10^6$	$9.9181 \cdot 10^{-1}$
$-1.9877 \cdot 10^7$	$9.4665 \cdot 10^{-1}$
$-1.7198 \cdot 10^8$	$6.8759 \cdot 10^{-1}$
$1.1471 \cdot 10^9$	$-2.1564 \cdot 10^{-1}$

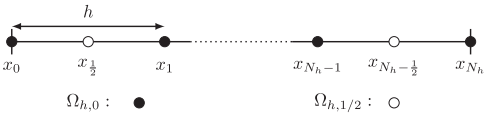

Fig. 5. Spatial discretization.

4. Time domain simulation with discrete-time constitutive relation

The objective of the present section is to integrate previously obtained discrete-time material law into an efficient finite-difference numerical scheme, in order to solve problems defined by Eqs. (1).

4.1. Explicit finite difference scheme

We start by keeping the same time discretization (time step Δt, sampling frequency $f_s = \Delta t^{-1}$) as the one introduced in Section 2.2. In order to represent the constitutive Eq. (1a), we use the discrete-time framework introduced in the previous section and transpose the transfer function (7) in the time domain, where z^{-1} stands for the unit delay operator ($z^{-1}\mathrm{TZ}(v^n) = \mathrm{TZ}(v^{n-1})$). We obtain a discrete time-domain constitutive law involving N_f internal variables $\sigma_k^n(x)$ at t^n. Furthermore, we choose to approximate Eq. (1b) by a leap-frog scheme, which is explicit and second order in time. Thus, the semi-discretized problem in time writes

$$\begin{aligned}
&\sigma_k^{n+1}(x) = H_{0k}\frac{du^{n+1}}{dx}(x) + p_k\sigma_k^n(x), \quad k = \{1, \ldots, N_f\},\\
&\sigma^{n+1}(x) = H_0\frac{du^{n+1}}{dx}(x) + \sum_{k=1}^{N_f}\sigma_k^{n+1}(x),
\end{aligned} \tag{23a}$$

$$\rho(x)\frac{u^{n+1}(x) - 2u^n(x) + u^{n-1}(x)}{\Delta t^2} = \frac{d\sigma^n(x)}{dx} + f^n(x). \tag{23b}$$

Regarding the spatial discretization (Fig. 5), we divide the interval $[0, L]$ with $N_h + 1$ points of equal step $h = L/N_h$ to obtain a first grid $\Omega_{h,0}$ of points $x_j = jh$. At time t^n, we introduce the values u_j^n and f_j^n of u and f on points x_j, and the corresponding vectors $\mathbf{u}_h^n$ and $\mathbf{f}_h^n$. We also introduce a staggered grid $\Omega_{h,1/2}$ of points $x_{j+(1/2)}$ on which we define the values $\sigma_{j+(1/2)}^n$ and $\varepsilon_{j+(1/2)}^n$, and the corresponding vectors $\boldsymbol{\sigma}_h^n$ and $\boldsymbol{\varepsilon}_h^n$. For any discrete field $\mathbf{v}_h^n$ (resp. $\mathbf{w}_h^n$) defined on $\Omega_{h,0}$ (resp. $\Omega_{h,1/2}$), we introduce the operator $\mathbf{D}_h$ (resp. $\mathbf{D}_h^*$) of second-order centered spatial derivative defined on $\Omega_{h,1/2}$ (resp. $\Omega_{h,0}$):

$$\mathbf{D}_h\mathbf{v}_h^n = \left[\frac{v_{j+1}^n - v_j^n}{h}\right]_j \in \Omega_{h,1/2}, \quad \mathbf{D}_h^*\mathbf{w}_h^n = \left[\frac{w_{j+(1/2)}^n - w_{j-(1/2)}^n}{h}\right]_j \in \Omega_{h,0}. \tag{24}$$

Finally, the full-discretized explicit problem writes

$$\begin{aligned}
&\boldsymbol{\sigma}_{hk}^{n+1} = H_{0k}\mathbf{D}_h\mathbf{u}_h^{n+1} + p_k\boldsymbol{\sigma}_{hk}^n, \quad k = \{1, \ldots, N_f\},\\
&\boldsymbol{\sigma}_h^{n+1} = H_0\mathbf{D}_h\mathbf{u}_h^{n+1} + \sum_{k=1}^{N_f}\boldsymbol{\sigma}_{hk}^{n+1},
\end{aligned} \tag{25a}$$

$$\rho\frac{\mathbf{u}_h^{n+1} - 2\mathbf{u}_h^n + \mathbf{u}_h^{n-1}}{\Delta t^2} = \mathbf{D}_h^*\boldsymbol{\sigma}_h^n + \mathbf{f}_h^n. \tag{25b}$$

4.2. Discrete energy and stability analysis

An interesting way to study the behavior of a numerical time-integration scheme is to investigate its ability to preserve a discrete energy across the time steps of the simulation [6]. Let us note that such a study has been performed in [18] for a discretized system with a generalized Zener model. The same approach has been applied to the present scheme where the material law is represented by a digital filter. For the sake of clarity, only the results of the energetic analysis and the subsequent stability analysis will be exposed in the current section and we refer to the Appendix A for the corresponding developments. In particular, notations $\|\cdot\|_0$, $\|\cdot\|_{1/2}$ and $(\cdot,\cdot)_0$, $(\cdot,\cdot)_{1/2}$ refer to particular norms and scalar products detailed in Eqs. (A.2a) and (A.2b).

Studying scheme (25) enables us to express the following energy identity:

$$\frac{E_h^{n+(1/2)} - E_h^{n-(1/2)}}{\Delta t} = P_h^n - D_h^n, \tag{26}$$

which relates the variation of the numerical energy $E_h^{n+(1/2)}$ between time steps $t^{n-(1/2)}$ and $t^{n+(1/2)}$ to the work of the external forces P_h^n and the dissipation D_h^n arising from one-pole filters at time step t^n. This identity makes use of internal variables $\mathbf{s}_{hk}^n$, which are related to the dissipative part of each one-pole filter:

$$\mathbf{s}_{hk}^n = \boldsymbol{\sigma}_{hk}^n - \frac{H_{0k}}{1-p_k}\mathbf{D}_h\mathbf{u}_h^n, \quad k=\{1,\ldots,N_f\}. \tag{27}$$

In the previous energy identity (26), $E_h^{n+(1/2)}$ may be split in three distinct terms $E_{hk}^{n+(1/2)}$, $E_{hf}^{n+(1/2)}$ and $E_{hs}^{n+(1/2)}$:

$$E_h^{n+(1/2)} = E_{hk}^{n+(1/2)} + E_{hf}^{n+(1/2)} + E_{hs}^{n+(1/2)}, \tag{28a}$$

with

$$E_{hk}^{n+(1/2)} = \frac{\rho}{2}\left\|\frac{\mathbf{u}_h^{n+1}-\mathbf{u}_h^n}{\Delta t}\right\|_0^2, \tag{28b}$$

$$E_{hf}^{n+(1/2)} = \frac{1}{2}\left(H_0 + \sum_{k=1}^{N_f}\frac{H_{0k}}{1-p_k}\right)(\mathbf{D}_h\mathbf{u}_h^{n+1}, \mathbf{D}_h\mathbf{u}_h^n)_{1/2} - \sum_{k=1}^{N_f}\frac{1-p_k^2}{8H_{0k}p_k}\left(\|\mathbf{s}_{hk}^{n+1}\|_{1/2}^2 + \|\mathbf{s}_{hk}^n\|_{1/2}^2\right), \tag{28c}$$

$$E_{hs}^{n+(1/2)} = -\frac{\Delta t^2}{4}\sum_{k=1}^{N_f}\left(\frac{\mathbf{s}_{hk}^{n+1}-\mathbf{s}_{hk}^n}{\Delta t}, \mathbf{D}_h\left(\frac{\mathbf{u}_h^{n+1}-\mathbf{u}_h^n}{\Delta t}\right)\right)_{1/2}. \tag{28d}$$

The first term $E_{hk}^{n+(1/2)}$ corresponds to the discrete kinetic energy of the system, while the second term $E_{hf}^{n+(1/2)}$ is related to the discrete internal energy stored in the digital filter. Finally, the last term $E_{hs}^{n+(1/2)}$ comes from the finite difference approximation. In the right-hand side of Eq. (26), the dissipation D_h^n, which involves mean values of $\mathbf{s}_{hk}$ between time steps, is simply the sum of the dissipation terms associated to each one-pole filter:

$$D_h^n = -\sum_{k=1}^{N_f}\frac{(1-p_k)^2}{2\Delta t H_{0k}p}\left[\left\|\frac{\mathbf{s}_{hk}^{n+1}+\mathbf{s}_{hk}^n}{2}\right\|_{1/2}^2 + \left\|\frac{\mathbf{s}_{hk}^n+\mathbf{s}_{hk}^{n-1}}{2}\right\|_{1/2}^2\right]. \tag{28e}$$

Finally, the work of the external forces is expressed as

$$P_h^n = \left(\mathbf{f}_h^n, \frac{\mathbf{u}_h^{n+1}-\mathbf{u}_h^{n-1}}{2\Delta t}\right)_0. \tag{28f}$$

On the basis of the previous energetic identity, we study the conditions which ensure that the discrete energy $E_h^{n+(1/2)}$ and the dissipation term D_h^n remains positive for each time step. Assuming the necessary condition (6) on the poles p_k enabling causality and stability of the filter is fulfilled, this leads to additional sufficient conditions involving filter coefficients and filter response $H(z)$ at a specific point:

$$H(1) \geq 0, \tag{29a}$$

$$H_{0k}p_k \leq 0, \quad k=\{1,\ldots,N_f\}; \tag{29b}$$

as well as discretization parameters:

$$\Delta t \leq h\sqrt{\frac{\rho}{H(-1)}}. \tag{29c}$$

It is worth noting that the filter representing a material law has to be synthesized prior to the simulation process at a selected sampling frequency f_s, which therefore fixes the time step Δt used for the simulation: $\Delta t = f_s^{-1}$. Consequently, it is more interesting to express previous stability condition in terms of the sampling frequency and continuous frequency response of the filter:

$$H^c(0) \geq 0, \tag{30a}$$

$$H_{0k}p_k \leq 0, \quad k=\{1,\ldots,N_f\}, \tag{30b}$$

$$h \geq h_{\min} = \frac{1}{f_s}\sqrt{\frac{H^c(\pi f_s)}{\rho}}. \tag{30c}$$

So far, it is interesting to note that the two first conditions (30a) and (30b) are exactly the same as (16) and (18) introduced in Section 2.4, which both ensure the positivity of the static modulus and the dissipative behavior of each one-pole sub-filter involved in the discrete behavior law. At last, the third condition (30c) is a classic CFL stability condition on the space discretization parameter h that involves the response of filter H^c at the Nyquist frequency $\omega = \pi f_s$ or $f = f_s/2$, which is the

maximum valid frequency associated to the sampling rate f_s. Indeed, the ratio $\sqrt{H^c(\pi f_s)/\rho}$ may be interpreted as the maximum speed of longitudinal waves traveling into the medium.

4.3. Dispersion and dissipation analysis

Dispersion and dissipation properties are essential features of numerical schemes in the simulation of wave propagation phenomena. Unfortunately, although the literature contains a large numbers of works for conservative systems, there seems to be only few works devoted to the study of dissipative systems, among which the work by Robertsson et al. [29].

A first step to investigate the dispersion and dissipation properties of our numerical scheme is to determine the associated dispersion relation. To do so, we follow a classical procedure and consider a single wave solution of the form:

$$\mathbf{u}_h^n = \left[w^n \exp(ijk_h^* h)\right]_j \quad (\text{with } i=\sqrt{-1}), \tag{31}$$

where k_h^* is the complex wavenumber of the discrete problem accounting for both dispersion and dissipation phenomena. We also extend the definition (3) of the Z-transform to the fields defined on $\Omega_{h,0}$ and $\Omega_{h,1/2}$ as

$$\text{TZ: } \{\mathbf{v}_h^n\}_n = \left\{\left[v_j^n\right]_j\right\}_n \longmapsto \check{\mathbf{v}}_h(z) = \left[\sum_{n=-\infty}^{\infty} \mathbf{v}_h^n z^{-n}\right]_j, \tag{32}$$

such that the fundamental property $\text{TZ}(\mathbf{v}_h^{n+1}) = z\text{TZ}(\mathbf{v}_h^n)$ holds.

Then, applying the Z-transform to Eq. (25), where the external forces are taken equal to zero, gives

$$\check{\boldsymbol{\sigma}}_{hk}(z)(1-p_k z^{-1}) = H_{0k}\text{TZ}(\mathbf{D}_h\mathbf{u}_h^n), \quad k=\{1,\ldots,N_f\},$$

$$\check{\boldsymbol{\sigma}}_h(z) = H_0\text{TZ}(\mathbf{D}_h\mathbf{u}_h^n) + \sum_{k=1}^{N_f} \check{\boldsymbol{\sigma}}_{hk}(z), \tag{33a}$$

$$\rho\frac{z-2+z^{-1}}{\Delta t^2}\check{\mathbf{u}}_h(z) = \text{TZ}(\mathbf{D}_h^*\boldsymbol{\sigma}_h^n). \tag{33b}$$

From the linearity of TZ, one has $\text{TZ}(\mathbf{D}_h\mathbf{v}_h^n) = \mathbf{D}_h\check{\mathbf{v}}_h(z)$ and the same applies to $\mathbf{D}_h^*$, such that Eq. (33) may be rewritten involving discrete transfer function $H(z)$ by substituting (33a) and (33b):

$$\rho\check{\delta}_{t\cdot}(z)\check{\mathbf{u}}_h(z) = H(z)\mathbf{D}_h^*\mathbf{D}_h\check{\mathbf{u}}_h(z), \tag{34}$$

where $\check{\delta}_{t\cdot}(z)$ denotes the Z transform of the leap-frog (25b):

$$\check{\delta}_{t\cdot}(z) = \frac{z-2+z^{-1}}{\Delta t^2}. \tag{35}$$

Next, using the discrete-time-space ansatz (31) leads to

$$\mathbf{D}_h^*\mathbf{D}_h\check{\mathbf{u}}_h(z) = \frac{\exp(ik_h^*h)-2+\exp(-ik_h^*h)}{h^2}\check{\mathbf{u}}_h(z) = -\frac{4}{h^2}\sin^2\left(\frac{k_h^*h}{2}\right)\check{\mathbf{u}}_h(z),$$

so that Eq. (34) becomes

$$\rho\check{\delta}_{t\cdot}(z) = -\frac{4}{h^2}H(z)\sin^2\left(\frac{k_h^*h}{2}\right). \tag{36}$$

Finally, the dispersion relation may be obtained by evaluating relation (36) on the unit circle, that is substituting z by $\exp(i\omega f_s^{-1})$ and observing that

$$\check{\delta}_{t\cdot}(\exp(i\omega f_s^{-1})) = -\frac{4}{\Delta t^2}\sin^2\left(\frac{\omega\Delta t}{2}\right).$$

As a result, we obtain the following dispersion relation:

$$k_h^*(\omega) = k_{hr}(\omega) + ik_{hi}(\omega) = \pm\frac{2}{h}\arcsin\left[\frac{h}{\Delta t}\sqrt{\frac{\rho}{H^c(\omega)}}\sin\left(\frac{\omega\Delta t}{2}\right)\right]. \tag{37}$$

From the real part k_{hr} and imaginary part k_{hi} of the discrete wave number, we also define the speed c_h and damping coefficient α_h associated with the discrete problem (25). To do so, we consider a continuous fictive solution u which may be written as

$$u(x,t) = u_0\exp(ik_h^*(\omega)x-\omega t) = u_0\exp(-k_{hi}(\omega)x)\exp(ik_{hr}(\omega)x-\omega t) = u_0\exp(-\alpha_h(\omega)t)\exp(ik_{hr}(\omega)(x-c_h(\omega)t),$$

with c_h and α_h defined as

$$c_h(\omega) = \frac{\omega}{k_{hr}(\omega)}, \quad \alpha_h(\omega) = c_h(\omega) k_{hi}(\omega) = \omega \frac{k_{hi}(\omega)}{k_{hr}(\omega)}. \tag{38}$$

5. Numerical simulations

Let us now illustrate on a simple example the whole approach, including both filter synthesis and simulation steps. To do so, we consider the model problem of Section 2.1 with a beam of length $L = 1$ m and density $\rho = 1149$ kg/m^3, constituted of the same material as the nylon bar specimen studied by Collet et al. [22] and excited by an impact on its right end. In order to build the discrete-time behavior, we consider the experimental data on complex modulus obtained in [22] and represented (with black dots) in Fig. 6.

In the following, we wish to simulate the response of the beam on the frequency range [20 Hz, 20 kHz] corresponding to audible signals, while ensuring given error criteria on dispersion and dissipation. Concerning sound perception, the most restrictive criterion has to be set on the dispersion error which will be limited to 1% as it corresponds to the order of magnitude of pitch sensitivity perceived by the human ear. The criterion on the dissipation error, which is related to the temporal decay of each harmonics, is less critical and will be set accordingly to 5%.

Next, in the present discrete-time behavior framework, the whole simulation process involves: (1) finding the best sampling frequency f_s, (2) identifying material law and (3) performing numerical simulation. However, choosing the best sampling frequency f_s from an error criterion on dispersion and dissipation of the numerical scheme is not an easy task since the validation of such criterion depends on the continuous response of the synthesized filter, as shown in Section 4.3, which itself requires f_s to be fixed prior to the optimization process, as shown in Section 3. Consequently, in order to minimize overall computational load, we suggest to set f_s to its lowest possible value through an iterative procedure that involves many filter synthesis followed by validation of dispersion and dissipation error criteria.

5.1. Filter synthesis

In the subsequent developments, for the sake of simplicity, we choose to fix the sampling frequency f_s *a priori* to 180 kHz, which is 9 times higher than the maximum frequency of the considered frequency range. Then, filter $\mathcal{H}$ is synthesized through constrained optimization problem (20), using GNU Octave `sqp` function in a same way as what has been done in Section 3.2. At the end of the process, one obtains a filter made of $N_f = 4$ one-pole sub-filter whose coefficients are detailed in Table 2 and whose frequency-domain response is plotted in Fig. 6. It must be emphasized that the synthesized filter can only represent the correct material behavior in the frequency range covered by the experimental values, i.e. 500 Hz to 8 kHz approximately. Outside this frequency range, the filter yields a physically possible behavior in terms of causality and verification of thermodynamics laws, but not necessarily the "correct" behavior for such materials. In the following, we set the frequency range of interest $[f_{\min}, f_{\max}]$ (introduced in Section 3.2) of the synthesis algorithm to [100 Hz, 20 kHz]. This frequency range thus goes beyond the frequency range covered by the experimental values of Collet et al. [22].

5.2. Choice of excitation function

In order to highlight the influence of dispersion and dissipation due to the numerical scheme during the time-domain simulation, it is desirable to use a broadband excitation with small low frequency components. Thus, we choose to model

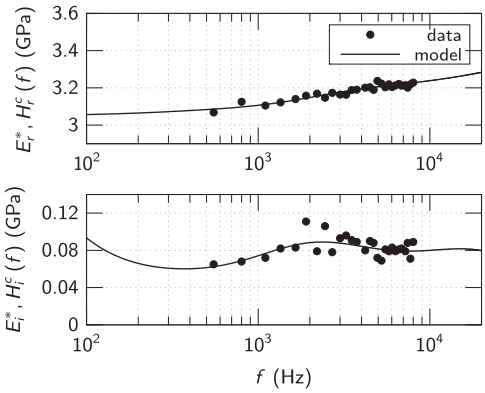

Fig. 6. Real (top) and imaginary (bottom) parts of experimental data (solid circles) related to the nylon bar specimen of [22] and response H^c of the synthesized digital filter (solid curves) with pure gain and $N_f = 4$ one-pole sub-filters.

the impact time function by a Ricker wavelet given by

$$F(t) = F_0\left(1-2\pi^2 f_0^2 (t-t_0)^2\right)\exp\left(-\pi^2 f_0^2 (t-t_0)^2\right), \tag{39}$$

where f_0 is the maximum of the frequency spectrum, fixed to 10 kHz, and $F_0 = 1.0 \times 10^{11}$ N/m^2. Fig. 7 shows the time-domain shape and the power spectral density of such an excitation.

Let us note that all power spectral densities presented here are given in terms of normalized power level in dB, which writes for a given signal $\hat{v}(f)$ as

$$L_V^N = 20\log_{10}\left(\frac{\hat{v}(f)}{\max\limits_f \hat{v}(f)}\right). \tag{40}$$

5.3. Time-domain simulation

Once the filter has been synthesized, numerical simulation of the resulting discrete problem (25) is performed keeping the same time discretization corresponding to the sampling frequency f_s. Then, the CFL condition (30c) associated with the explicit scheme (25) gives the minimum value $h_{\min}$ of the spatial discretization parameter h in order to guarantee the stability of the numerical scheme. Next, mesh size is chosen as the minimum value $h \geq h_{\min}$ which remains compatible with the uniform spatial discretization of the beam, which yields (denoting $E(Y)$ the integer part of Y):

$$h = \frac{L}{N_h} \quad \text{with} \quad N_h = E\left(\frac{L}{h_{\min}}\right)+1. \tag{41}$$

Furthermore, it is interesting to note from (30c) the proportionality relation between $h_{\min}$ and $\sqrt{H^c(\pi f_s)}$, which suggests to keep this last value as small as possible during the optimization process in order to lower the spatial discretization step. This may be particularly relevant when working in a frequency range $[f_{\min}, f_{\max}]$ that is far from $f_s/2$, where the optimization process may leads to a significant increase of H^c between $f_{\max}$ and $f_s/2$ without noticeable improvement of the material response on the frequency range of interest. This last remark may be taken into account by directly incorporating an additional constraint $H^c(\pi f_s) \leq H^c_{\max}$ in the optimization process (20).

In order to study the influence of h on the properties of the numerical scheme, let us introduce the following CFL number as $\mathrm{CFL} = h/h_{\min}$, such that $\mathrm{CFL} = 1$ in the ideal case corresponding to $h = h_{\min}$. As for the present problem, the minimum possible spatial size is $h = 9.52$ mm which corresponds to a CFL number of 1.004. The time evolution of beam displacement u at observation point $x_{\mathrm{obs}} = 0.47L$ is plotted in Fig. 8. Fig. 9 plots both the associated power spectral density L_U^N and phase φ_U for the two CFL numbers and compares it to a reference modal solution detailed in Appendix B. These two figures show that the numerical solution agrees very well with the modal one over the whole frequency band for the best CFL value of 1.004, whereas one may clearly notice some discrepancies increasing with frequency for a CFL value of 1.110.

Table 2
Coefficients of synthesized filter $\mathcal{H}$ related to nylon for $N_f = 4$.

$H_0, H_{0,k}$	p_k
$3.4299 \cdot 10^9$	
$-2.8670 \cdot 10^5$	$9.8987 \cdot 10^{-1}$
$-2.7138 \cdot 10^5$	$9.9991 \cdot 10^{-1}$
$-1.0050 \cdot 10^7$	$9.2889 \cdot 10^{-1}$
$-1.0941 \cdot 10^8$	$4.6631 \cdot 10^{-1}$

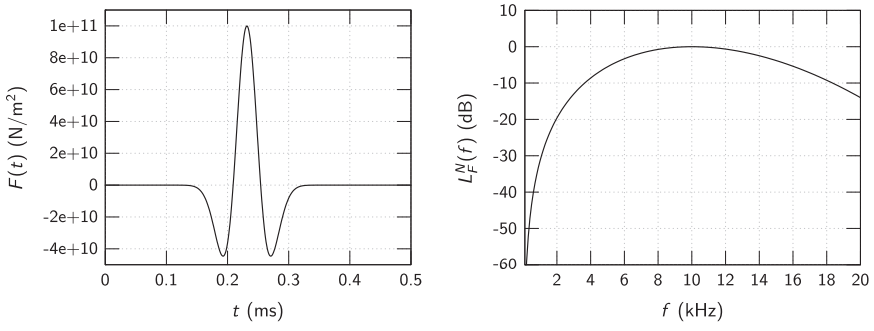

Fig. 7. Time-domain evolution (left) and normalized power spectral density (right) of Ricker wavelet excitation $F(t)$ with $f_0 = 10$ kHz.

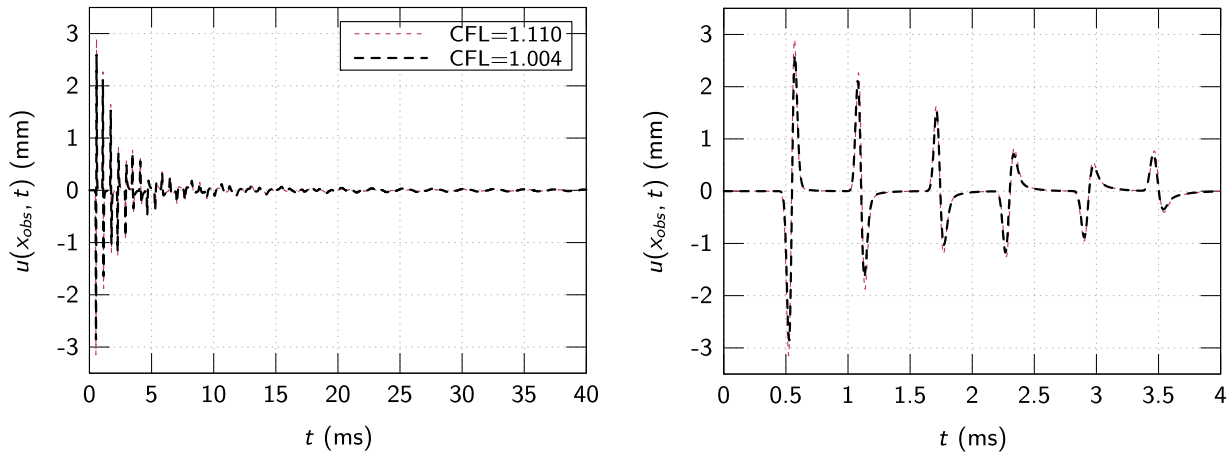

Fig. 8. Time-domain response $u(x_{obs}, t)$ corresponding to CFL = 1.004 (black thick dashed) and CFL = 1.110 (magenta thin dashed) up to 40 ms (left) and up to 4 ms (right). (For interpretation of the references to color in this figure caption, the reader is referred to the web version of this paper.)

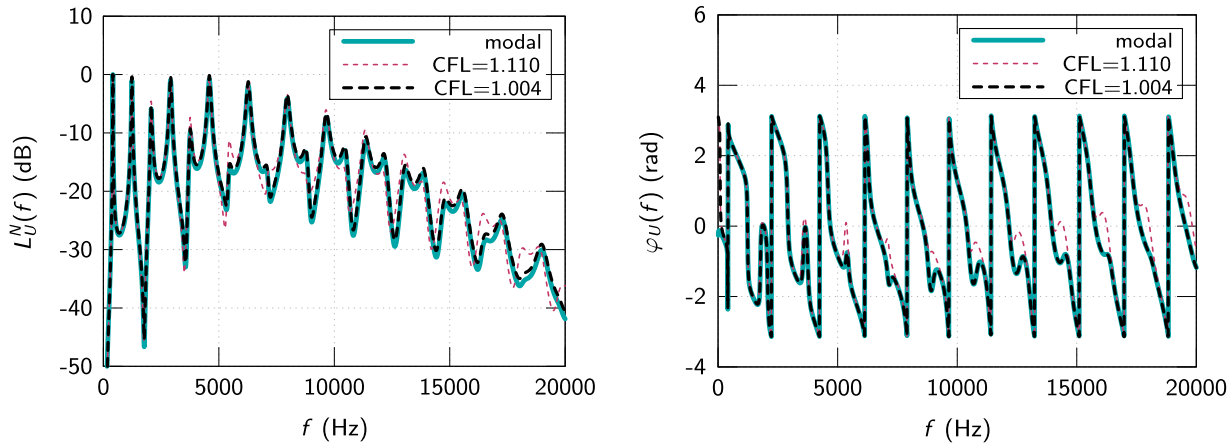

Fig. 9. Power spectral density L_U^N in log level (left) and phase response φ_U (right) corresponding to CFL=1.004 (black thick dashed), CFL=1.110 (magenta thin dashed) and reference solution (cyan thick solid). (For interpretation of the references to color in this figure caption, the reader is referred to the web version of this paper.)

Now, in order to illustrate the performance of the scheme relative to dispersion and dissipation, we introduce the relative errors e_r^k and e_i^k on numerical dispersion and dissipation by

$$e_r^k(\omega) = \frac{|k_r(\omega) - k_{hr}(\omega)|}{|k_r(\omega)|}, \quad e_i^k(\omega) = \frac{|k_i(\omega) - k_{hi}(\omega)|}{|k_i(\omega)|}, \tag{42}$$

where k_{hr} and k_{hi} are defined from dispersion analysis of Section 4.3 and k_r and k_i are related to the complex number of the reference problem. Fig. 10 shows relatives errors e_r^k and e_i^k on the real and imaginary part of the wavenumber for the ideal case corresponding to CFL=1 (solid curve) and for the lower admissible spatial discretization corresponding to CFL=1.004 (dashed curve). We notice that the error e_r^k, which may be linked to the speed of waves propagating into the medium, remains lower than 1% over the whole frequency range of interest. However, comparing it with the ideal curve shows an important variation of e_r^k close to $f_s/2$ despite a very low increase of the CFL coefficient. As for the imaginary part of the wavenumber, it is noticeable that the relative error is an order of magnitude greater. However, we notice that the increase of CFL number has less influence here, the two corresponding curves being very close. Hence, the dissipation error seems to come essentially from the numerical scheme itself and little from the choice of discretization parameters, which suggest to use fourth order schemes in the time discretization of Eq. (1b) and in the definition of spatial operators (24) in order to reduce it. Here, optimal choice of h corresponding to CFL=1.004 leads to a relative error of 0.06% for e_r^k and 4.46% for e_i^k at 20 kHz, which validates *a posteriori* the initial choice of f_s regarding error criterions introduced in the beginning of the section.

Starting from the dispersion relation, one can express the wavelength λ as a function of the frequency f for the continuous reference problem by

$$\lambda(f) = c(f) f^{-1} = \frac{\mathcal{R}e(H^c(f))}{f\sqrt{\rho}}. \tag{43}$$

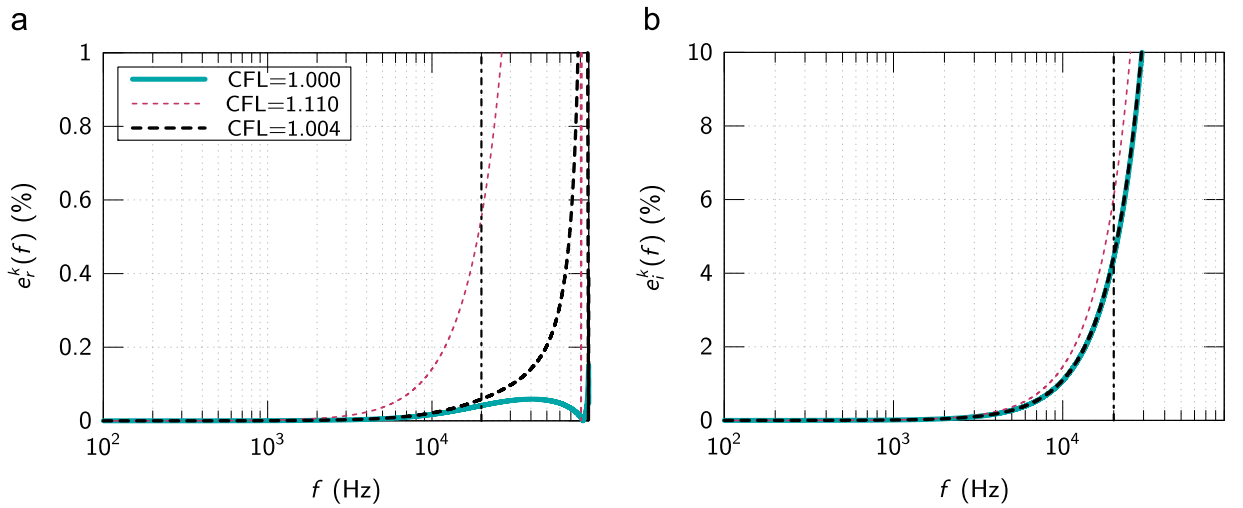

Fig. 10. Dispersion and dissipation properties corresponding to CFL=1 (cyan thick solid), CFL=1.004 (black thick dashed) and CFL=1.110 (magenta thin dashed) on the frequency range $[f_{\min}, f_s/2]$, where the maximum frequency of interest $f_{\max} = 20$ kHz is shown by dashed black line. (a) Dispersion error $e_r^k(\omega)$. (b) Dissipation error $e_i^k(\omega)$. (For interpretation of the references to color in this figure caption, the reader is referred to the web version of this paper.)

The space discretization parameter h may then be compared to the smallest wavelength $\lambda_{\min}$ in the frequency range of interest, that is $\lambda_{\min} = 84.53$ mm corresponding to $f = 20$ kHz. Such a discretization corresponds to a minimal spatial resolution of 8 points per wavelength.

At last, in order to study how the spatial discretization factor h may influences the quality of the final solution, especially regarding dispersion and dissipation errors, an additional simulation has been performed for $h = 10.53$ mm, corresponding to a CFL coefficient of 1.110. As it can be seen in Fig. 10, the dispersion error is very sensitive to the increase of CFL number, which is in agreement with previous comments. Indeed, relative error e_r^k reaches 0.55% at CFL=1.110 and its influence is noticeable in Fig. 9 from about 12 kHz. As for the dissipation, the increase of the relative error is also significant with e_i^k reaching 6.06%, which leads to an underestimation of damping on the higher frequency range. This last point is also noticeable with overruns located on the peaks of the time-domain responses plotted in Fig. 8.

6. Conclusion

The work that has been presented in this paper introduces an original approach to provide well-posed and accurate description of damping phenomena for various materials in the context of time-domain numerical simulations. Its original feature is to build a discrete-time model which may be interpreted as a digital filter, thus allowing to use the common tools available in the field of digital filtering. The whole process including material identification and numerical simulation may be summarized by the following steps:

1. choose an initial sampling frequency f_s;
2. synthesize filter $\mathcal{H}$, representing discrete-time material law, from experimental data;
3. calculate minimum grid step $h_{\min}$ from $H^c(\pi f_s)$ using CFL relation (30c);
4. choose minimal grid step $h \geq h_{\min}$ compatible with geometric parameters;
5. compute dispersion and dissipation errors e_r^k and e_i^k over the frequency range and validate error criterion;
6. if previous validation fails, choose a refined sampling frequency $f_s' \geq f_s$ and restart steps 2–5 up to the satisfaction of error criterion.

The filter is synthesized through an optimization process in order to have its transfer function in the frequency domain approximate a given set of complex elastic moduli at various frequencies. Moreover, adding some constraints on the filter coefficients during the optimization process allows one to obtain a resulting discrete-time model satisfying stability, causality and positivity of dissipation. Finally, its transposition into the time domain is straightforward and leads to a recursive discrete-time relation which is directly implementable into a numerical integration scheme and may be interpreted as a discrete-time constitutive law with internal variables. Furthermore, the choice of the sub-filters constituting the filter previously synthesized, enable the whole numerical scheme resulting from the discrete-time constitutive law and the discretization of linear momentum equation to fulfill some discrete-time energetic identity. As a result, the whole modeling procedure may be interpreted as a two-way process which (1) carries identification of a continuous time-domain law from experimental results and (2) sets up the best time-discretization scheme in order to master the high-frequency discrepancies between continuous-time and discrete-time frequency response of the resulting model. Besides, one may

evaluate errors on dispersion and dissipation of the numerical scheme and control it through an optimal choice of both discretization and filter parameters having an impact on the high-frequency response of the discrete model.

Up to now, this approach has been developed on a one-dimensional problem with finite difference integration scheme in space and time. Future developments will deal with its integration into dynamic three dimensional problems with finite element discretization in space and finite difference time integration, and with extension to inhomogeneous and anisotropic materials. Also, the extension and theoretical analysis of the general form of the material filter with multiple and complex-conjugate poles will be done in future works.

Acknowledgments

The authors would like to thank the French "Direction Générale de l'Armement" (DGA) for supporting this work.

Appendix A. Energetic analysis and stability of integration scheme

In order to perform the energetic analysis of scheme (25), we first start by introducing the Hilbert spaces $L^2(\Omega_{h,0})$ et $L^2(\Omega_{h,1/2})$ defined as

$$L^2(\Omega_{h,0}) = \left\{ \mathbf{v}_h = [v_j]_{j=\{0,\dots,N_h\}} \in \Omega_{h,0},\ \sum_{j=0}^{N_h} |v_j|^2 < +\infty \right\}, \tag{A.1a}$$

$$L^2(\Omega_{h,1/2}) = \left\{ \mathbf{v}_h = [v_{j+(1/2)}]_{j=\{0,\dots,N_h-1\}} \in \Omega_{h,1/2},\ \sum_{j=0}^{N_h-1} |v_{j+(1/2)}|^2 < +\infty \right\}; \tag{A.1b}$$

together with the following associated discrete norms and scalar products:

$$\|\mathbf{v}_h\|_0 = \left[\sum_{j=0}^{N_x} h|v_j|^2 \right]^{1/2}, \quad (\mathbf{v}_h, \mathbf{w}_h)_0 = \sum_{j=0}^{N_x} h\, v_j w_j,\ \forall (\mathbf{v}_h, \mathbf{w}_h) \in L^2(\Omega_{h,0})^2, \tag{A.2a}$$

$$\|\mathbf{v}_h\|_{1/2} = \left[\sum_{j=0}^{N_x-1} h|v_{j+(1/2)}|^2 \right]^{1/2}, \quad (\mathbf{v}_h, \mathbf{w}_h)_{1/2} = \sum_{j=0}^{N_x-1} h\, v_{j+(1/2)} w_{j+(1/2)},\ \forall (\mathbf{v}_h, \mathbf{w}_h) \in L^2(\Omega_{h,1/2})^2. \tag{A.2b}$$

Let us note that $\mathbf{D}_h^*$ and $\mathbf{D}_h$ are skew-self-adjoint operators, such that

$$(\mathbf{v}_h, \mathbf{D}_h^* \mathbf{w}_h)_0 = -(\mathbf{D}_h \mathbf{v}_h, \mathbf{w}_h)_{1/2}, \quad \forall (\mathbf{v}_h, \mathbf{w}_h) \in L^2(\Omega_{h,0}) \times L^2(\Omega_{h,1/2}).$$

For the sake of simplicity, we perform the stability analysis on numerical schemes with increasing complexity, starting with a system with one pure gain filter, followed by a system with one-pole filter, before extending it to system (25) of multiple one-pole filters. Finally, this last energetic result allows us to derive the stability condition of scheme (25).

A.1. System with pure gain filter

We start by performing the energetic analysis of a simplified discrete problem where the material behavior is only constituted by a pure gain filter ($H(z) = H_0$), corresponding to a purely elastic case. Eq. (25a) becomes $\boldsymbol{\sigma}_h^n = H_0 \mathbf{D}_h \mathbf{u}_h^n$ and the discrete problem associated with this lossless system writes

$$\rho \frac{\mathbf{u}_h^{n+1} - 2\mathbf{u}_h^n + \mathbf{u}_h^{n-1}}{\Delta t^2} = H_0 \mathbf{D}_h^* \mathbf{D}_h \mathbf{u}_h^n + \mathbf{f}_h^n. \tag{A.3}$$

Next, the energetic identity is achieved by multiplying (A.3) by $(\mathbf{u}_h^{n+1} - \mathbf{u}_h^{n-1})/2\Delta t$, which is the second order centered approximation of $\partial u/\partial t$ at step t^n, and integrating it on the whole domain. Using the norms and scalar products previously introduced yields

$$\frac{\rho}{2\Delta t} \left[\left\| \frac{\mathbf{u}_h^{n+1} - \mathbf{u}_h^n}{\Delta t} \right\|_0^2 - \left\| \frac{\mathbf{u}_h^n - \mathbf{u}_h^{n-1}}{\Delta t} \right\|_0^2 \right] + H_0 \left(\mathbf{D}_h \mathbf{u}_h^n, \mathbf{D}_h \left(\frac{\mathbf{u}_h^{n+1} - \mathbf{u}_h^{n-1}}{2\Delta t} \right) \right)_{1/2} = \left(\mathbf{f}_h^n, \frac{\mathbf{u}_h^{n+1} - \mathbf{u}_h^{n-1}}{2\Delta t} \right)_0. \tag{A.4}$$

Then, one obtains the following energetic identity:

$$\frac{E_h^{n+(1/2)} - E_h^{n-(1/2)}}{\Delta t} = \left(\mathbf{f}_h^n, \frac{\mathbf{u}_h^{n+1} - \mathbf{u}_h^{n-1}}{2\Delta t} \right)_0, \tag{A.5}$$

where $E_h^{n+(1/2)}$ stands for the discrete energy of the system at time step $t^{n+(1/2)}$, which is defined as

$$E_h^{n+(1/2)} = \frac{\rho}{2}\left\|\frac{\mathbf{u}_h^{n+1}-\mathbf{u}_h^n}{\Delta t}\right\|_0^2 + \frac{H_0}{2}(\mathbf{D}_h\mathbf{u}_h^{n+1}, \mathbf{D}_h\mathbf{u}_h^n). \tag{A.6}$$

From a mechanical point of view, $E_h^{n+(1/2)}$ stands for the classical discrete energy corresponding to a purely elastic behavior [18], and identity (A.5) simply expresses that its variation between time steps $t^{n-(1/2)}$ and $t^{n+(1/2)}$ is equal to the power of external forces $\mathbf{f}_h^n$ at time step t^n.

A.2. System with one-pole filter

Now, let us consider the case of a simplified discrete problem where the material behavior is only constituted by a one-pole filter:

$$\boldsymbol{\sigma}_h^{n+1} = H_0\mathbf{D}_h\mathbf{u}_h^{n+1} + p\boldsymbol{\sigma}_h^n, \tag{A.7a}$$

$$\rho\frac{\mathbf{u}_h^{n+1}-2\mathbf{u}_h^n+\mathbf{u}_h^{n-1}}{\Delta t^2} = \mathbf{D}_h^*\boldsymbol{\sigma}_h^n + \mathbf{f}_h^n. \tag{A.7b}$$

First of all, we introduce the internal variable $\mathbf{s}_h^n$ as

$$\mathbf{s}_h^n = \boldsymbol{\sigma}_h^n - \frac{H_0}{1-p}\mathbf{D}_h\mathbf{u}_h^n, \tag{A.8}$$

in order to rewrite System (A.7) in terms of $\mathbf{s}_h^n$:

$$\frac{1-p}{2}(\mathbf{s}_h^{n+1}+\mathbf{s}_h^n) + \frac{1+p}{2}(\mathbf{s}_h^{n+1}-\mathbf{s}_h^n) = -\frac{H_0 p}{1-p}\mathbf{D}_h(\mathbf{u}_h^{n+1}-\mathbf{u}_h^n). \tag{A.9a}$$

$$\rho\frac{\mathbf{u}_h^{n+1}-2\mathbf{u}_h^n+\mathbf{u}_h^{n-1}}{\Delta t^2} = \mathbf{D}_h^*\mathbf{s}_h^n + \frac{H_0}{1-p}\mathbf{D}_h^*\mathbf{D}_h\mathbf{u}_h^n + \mathbf{f}_h^n. \tag{A.9b}$$

Next, one multiplies (A.9a) by $(\mathbf{s}_h^{n+1}+\mathbf{s}_h^n)/2$ and integrates over the whole domain, while processing equilibrium equation (A.9b) in a similar way as for the lossless System (A.4), which yields:

$$\frac{1-p}{2}\left(\mathbf{s}_h^{n+1}+\mathbf{s}_h^n, \frac{\mathbf{s}_h^{n+1}+\mathbf{s}_h^n}{2}\right)_{1/2} + \frac{1+p}{2}\left(\mathbf{s}_h^{n+1}-\mathbf{s}_h^n, \frac{\mathbf{s}_h^{n+1}+\mathbf{s}_h^n}{2}\right)_{1/2} = -\frac{H_0 p}{1-p}\left(\mathbf{D}_h(\mathbf{u}_h^{n+1}-\mathbf{u}_h^n), \frac{\mathbf{s}_h^{n+1}+\mathbf{s}_h^n}{2}\right)_{1/2}, \tag{A.10a}$$

$$\begin{aligned}&\frac{\rho}{2\Delta t}\left[\left\|\frac{\mathbf{u}_h^{n+1}-\mathbf{u}_h^n}{\Delta t}\right\|_0^2 - \left\|\frac{\mathbf{u}_h^n-\mathbf{u}_h^{n-1}}{\Delta t}\right\|_0^2\right] + \left(\mathbf{s}_h^n, \mathbf{D}_h\left(\frac{\mathbf{u}_h^{n+1}-\mathbf{u}_h^{n-1}}{2\Delta t}\right)\right)_{1/2}\\ &+\frac{H_0}{1-p}\left(\mathbf{D}_h\mathbf{u}_h^n, \mathbf{D}_h\left(\frac{\mathbf{u}_h^{n+1}-\mathbf{u}_h^{n-1}}{2\Delta t}\right)\right)_{1/2} = \left(\mathbf{f}_h^n, \frac{\mathbf{u}_h^{n+1}-\mathbf{u}_h^{n-1}}{2\Delta t}\right)_0.\end{aligned} \tag{A.10b}$$

Taking the average of Eq. (A.10a) between time steps $t^{n-(1/2)}$ and $t^{n+(1/2)}$ gives

$$\begin{aligned}&\frac{1+p}{4}\left[\left(\mathbf{s}_h^{n+1}-\mathbf{s}_h^n, \frac{\mathbf{s}_h^{n+1}+\mathbf{s}_h^n}{2}\right)_{1/2} + \left(\mathbf{s}_h^n-\mathbf{s}_h^{n-1}, \frac{\mathbf{s}_h^n+\mathbf{s}_h^{n-1}}{2}\right)_{1/2}\right] + \frac{1-p}{2}\left[\left\|\frac{\mathbf{s}_h^{n+1}+\mathbf{s}_h^n}{2}\right\|_{1/2}^2 + \left\|\frac{\mathbf{s}_h^n+\mathbf{s}_h^{n-1}}{2}\right\|_{1/2}^2\right]\\ &= -\frac{H_0 p}{2(1-p)}\left[\left(\mathbf{D}_h(\mathbf{u}_h^{n+1}-\mathbf{u}_h^n), \frac{\mathbf{s}_h^{n+1}+\mathbf{s}_h^n}{2}\right)_{1/2} + \left(\mathbf{D}_h(\mathbf{u}_h^n-\mathbf{u}_h^{n-1}), \frac{\mathbf{s}_h^n+\mathbf{s}_h^{n-1}}{2}\right)_{1/2}\right].\end{aligned} \tag{A.11}$$

Besides, noticing that

$$\begin{aligned}&\left(\mathbf{D}_h(\mathbf{u}_h^{n+1}-\mathbf{u}_h^n), \frac{\mathbf{s}_h^{n+1}+\mathbf{s}_h^n}{2}\right)_{1/2} + \left(\mathbf{D}_h(\mathbf{u}_h^n-\mathbf{u}_h^{n-1}), \frac{\mathbf{s}_h^n+\mathbf{s}_h^{n-1}}{2}\right)_{1/2} = 1/2\Big[(\mathbf{D}_h(\mathbf{u}_h^{n+1}-\mathbf{u}_h^n), \mathbf{s}_h^{n+1}-\mathbf{s}_h^n)_{1/2}\\ &-(\mathbf{D}_h(\mathbf{u}_h^n-\mathbf{u}_h^{n-1}), \mathbf{s}_h^n-\mathbf{s}_h^{n-1})_{1/2}\Big] + (\mathbf{D}_h(\mathbf{u}_h^{n+1}-\mathbf{u}_h^{n-1}), \mathbf{s}_h^n)_{1/2},\end{aligned}$$

Eq. (A.11) may be rewritten as a function of $(\mathbf{s}_h^n, \mathbf{D}_h((\mathbf{u}_h^{n+1}-\mathbf{u}_h^{n-1})/2\Delta t))_{1/2}$:

$$\begin{aligned}&-\frac{1-p^2}{8H_0 p\Delta t}\left[(\mathbf{s}_h^{n+1}-\mathbf{s}_h^n, \mathbf{s}_h^{n+1}+\mathbf{s}_h^n)_{1/2} + (\mathbf{s}_h^n-\mathbf{s}_h^{n-1}, \mathbf{s}_h^n+\mathbf{s}_h^{n-1})_{1/2}\right] - \frac{(1-p)^2}{2H_0 p\Delta t}\left[\left\|\frac{\mathbf{s}_h^{n+1}+\mathbf{s}_h^n}{2}\right\|_{1/2}^2 + \left\|\frac{\mathbf{s}_h^n+\mathbf{s}_h^{n-1}}{2}\right\|_{1/2}^2\right]\\ &-\frac{1}{4\Delta t}\left[(\mathbf{D}_h(\mathbf{u}_h^{n+1}-\mathbf{u}_h^n), \mathbf{s}_h^{n+1}-\mathbf{s}_h^n)_{1/2} - (\mathbf{D}_h(\mathbf{u}_h^n-\mathbf{u}_h^{n-1}), \mathbf{s}_h^n-\mathbf{s}_h^{n-1})_{1/2}\right] = \left(\mathbf{s}_h^n, \mathbf{D}_h\left(\frac{\mathbf{u}_h^{n+1}-\mathbf{u}_h^{n-1}}{2\Delta t}\right)\right)_{1/2}.\end{aligned} \tag{A.12}$$

The last step consists in substituting Eq. (A.12) into Eq. (A.10b). This yields to the energetic identity associated to the one-pole system (A.7):

$$\frac{E_h^{n+(1/2)}-E_h^{n-(1/2)}}{\Delta t}=P_h^n-D_h^n, \tag{A.13}$$

where P_h^n and D_h^n are expressed as

$$P_h^n=\left(\mathbf{f}_h^n,\frac{\mathbf{u}_h^{n+1}-\mathbf{u}_h^{n-1}}{2\Delta t}\right)_0, \tag{A.14a}$$

$$D_h^n=-\frac{(1-p)^2}{2\Delta t H_0 p}\left[\left\|\frac{\mathbf{s}_h^{n+1}+\mathbf{s}_h^n}{2}\right\|_{1/2}^2+\left\|\frac{\mathbf{s}_h^n+\mathbf{s}_h^{n-1}}{2}\right\|_{1/2}^2\right], \tag{A.14b}$$

and the discrete energy $E^{n+(1/2)}$ at time step $t^{n+(1/2)}$ is now given by

$$E_h^{n+(1/2)}=\frac{\rho}{2}\left\|\frac{\mathbf{u}_h^{n+1}-\mathbf{u}_h^n}{\Delta t}\right\|_0^2+\frac{1}{2}\frac{H_0}{1-p}(\mathbf{D}_h\mathbf{u}_h^{n+1},\mathbf{D}_h\mathbf{u}_h^n)_{1/2}-\frac{1-p^2}{8H_0p}\left(\|\mathbf{s}_h^{n+1}\|_{1/2}^2+\|\mathbf{s}_h^n\|_{1/2}^2\right)-\frac{\Delta t^2}{4}\left(\frac{\mathbf{s}_h^{n+1}-\mathbf{s}_h^n}{\Delta t},\mathbf{D}_h\left(\frac{\mathbf{u}_h^{n+1}-\mathbf{u}_h^n}{\Delta t}\right)\right)_{1/2} \tag{A.14c}$$

Let us note that the previous energetic identity now involves an additional term D_h^n which stands for the dissipation associated with the discrete-time behavior (A.7a).

A.3. System with pure gain and multiple one-pole filters in parallel

The previous energy analysis detailed in Appendices A.1 and A.2 may be easily extended to the more general case corresponding to a discrete time-domain behavior given by the filter (7). Let us recall the associated discrete explicit problem as obtained in Section 4.1:

$$\boldsymbol{\sigma}_{hk}^{n+1}=H_{0k}\mathbf{D}_h\mathbf{u}_h^{n+1}+p_k\boldsymbol{\sigma}_{hk}^n,\quad k=\{1,\ldots,N_f\}, \tag{A.15a}$$

$$\boldsymbol{\sigma}_h^{n+1}=H_0\mathbf{D}_h\mathbf{u}_h^{n+1}+\sum_{k=1}^{N_f}\boldsymbol{\sigma}_{hk}^{n+1}, \tag{A.15b}$$

$$\rho\frac{\mathbf{u}_h^{n+1}-2\mathbf{u}_h^n+\mathbf{u}_h^{n-1}}{\Delta t^2}=\mathbf{D}_h^*\boldsymbol{\sigma}_h^n+\mathbf{f}_h^n. \tag{A.15c}$$

Similarly to what has been done in A.2 for a one-pole filter, one starts by defining the internal variables $\mathbf{s}_{hk}^n$ associated to each one-pole filter H_k:

$$\mathbf{s}_{hk}^n=\boldsymbol{\sigma}_{hk}^n-\frac{H_{0k}}{1-p_k}\mathbf{D}_h\mathbf{u}_h^n,\quad k=\{1,\ldots,N_f\}, \tag{A.16}$$

such that System (A.15) becomes

$$\frac{1-p_k}{2}(\mathbf{s}_{hk}^{n+1}+\mathbf{s}_{hk}^n)+\frac{1+p_k}{2}(\mathbf{s}_{hk}^{n+1}-\mathbf{s}_{hk}^n)\quad=-\frac{H_{0k}p_k}{1-p_k}\mathbf{D}_h(\mathbf{u}_h^{n+1}-\mathbf{u}_h^n),\quad k=\{1,\ldots,N_f\}, \tag{A.17a}$$

$$\rho\frac{\mathbf{u}_h^{n+1}-2\mathbf{u}_h^n+\mathbf{u}_h^{n-1}}{\Delta t^2}=\sum_{k=1}^{N_f}\mathbf{s}_{hk}^n+\left(H_0+\sum_{k=1}^{N_f}\frac{H_{0k}}{1-p_k}\right)\mathbf{D}_h^*\mathbf{D}_h\mathbf{u}_h^n+\mathbf{f}_h^n. \tag{A.17b}$$

Thereafter, each Eq. (A.17a) is processed independently for each k in a similar way as done in A.2, while Eq. (A.17b) is processed in a similar way as done in A.1.

Finally, combining all the terms gives the same type of energetic identity as (A.13)

$$\frac{E_h^{n+(1/2)}-E_h^{n-(1/2)}}{\Delta t}=P_h^n-D_h^n,$$

where D_h^n and $E^{n+(1/2)}$ now involve the sum of the terms associated to each one-pole filter while P_h^n remains the same as in (A.14a):

$$D_h^n=-\sum_{k=1}^{N_f}\frac{(1-p_k)^2}{2\Delta t H_{0k}p_k}\left[\left\|\frac{\mathbf{s}_{hk}^{n+1}+\mathbf{s}_{hk}^n}{2}\right\|_{1/2}^2+\left\|\frac{\mathbf{s}_{hk}^n+\mathbf{s}_{hk}^{n-1}}{2}\right\|_{1/2}^2\right], \tag{A.18a}$$

$$E_h^{n+(1/2)} = \frac{\rho}{2}\left\|\frac{\mathbf{u}_h^{n+1}-\mathbf{u}_h^n}{\Delta t}\right\|_0^2 + \frac{1}{2}\left(H_0 + \sum_{k=1}^{N_f}\frac{H_{0k}}{1-p_k}\right)(\mathbf{D}_h\mathbf{u}_h^{n+1}, \mathbf{D}_h\mathbf{u}_h^n)_{1/2} - \sum_{k=1}^{N_f}\frac{1-p_k^2}{8H_{0k}p_k}\left(\|\mathbf{s}_{hk}^{n+1}\|_{1/2}^2 + \|\mathbf{s}_{hk}^n\|_{1/2}^2\right) - \frac{\Delta t^2}{4}\sum_{k=1}^{N_f}\left(\frac{\mathbf{s}_{hk}^{n+1}-\mathbf{s}_{hk}^n}{\Delta t}, \mathbf{D}_h\left(\frac{\mathbf{u}_h^{n+1}-\mathbf{u}_h^n}{\Delta t}\right)\right)_{1/2} \tag{A.18b}$$

A.4. Stability analysis

In order to perform the stability analysis of the scheme (25), we study the conditions on the filter coefficients and discretization parameters which ensure that the discrete energy $E_h^{n+(1/2)}$ and dissipation D_h^n in Eq. (A.13) remain positive at each time step. Furthermore, we assume in the following that the condition (6) on the filter poles p_k is fulfilled.

First of all, let us rewrite Eq. (A.18b) using the following identities:

$$(\mathbf{D}_h\mathbf{u}_h^{n+1}, \mathbf{D}_h\mathbf{u}_h^n)_{1/2} = \frac{1}{4}\left(\|\mathbf{D}_h(\mathbf{u}_h^{n+1}+\mathbf{u}_h^n)\|_{1/2}^2 - \|\mathbf{D}_h(\mathbf{u}_h^{n+1}-\mathbf{u}_h^n)\|_{1/2}^2\right),$$

$$\left[\left(\|\mathbf{s}_h^{n+1}\|_{1/2}^2 + \|\mathbf{s}_h^n\|_{1/2}^2\right) - \left(\|\mathbf{s}_h^n\|_{1/2}^2 + \|\mathbf{s}_h^{n-1}\|_{1/2}^2\right)\right] = 1/2\left(\|\mathbf{s}_h^{n+1}+\mathbf{s}_h^n\|_{1/2}^2 + \|\mathbf{s}_h^{n+1}-\mathbf{s}_h^n\|_{1/2}^2\right)$$

$$-1/2\left(\|\mathbf{s}_h^n+\mathbf{s}_h^{n-1}\|_{1/2}^2 + \|\mathbf{s}_h^n-\mathbf{s}_h^{n-1}\|_{1/2}^2\right).$$

This enables to split the discrete energy $E_h^{n+(1/2)}$ at time step $t^{n+(1/2)}$ in two distinct terms $E_{h1}^{n+(1/2)}$ and $E_{h2}^{n+(1/2)}$:

$$E_h^{n+(1/2)} = E_{h1}^{n+(1/2)} + E_{h2}^{n+(1/2)}, \tag{A.19a}$$

which involve mean values and second order centered derivatives at $t^{n+(1/2)}$, respectively:

$$E_{h1}^{n+(1/2)} = \frac{1}{2}\left(H_0 + \sum_{k=1}^{N_f}\frac{H_{0k}}{1-p_k}\right)\left\|\mathbf{D}_h\left(\frac{\mathbf{u}_h^{n+1}+\mathbf{u}_h^n}{2}\right)\right\|_{1/2}^2 - \sum_{k=1}^{N_f}\frac{1-p_k^2}{4H_{0k}p_k}\left\|\frac{\mathbf{s}_{hk}^{n+1}+\mathbf{s}_{hk}^n}{2}\right\|_{1/2}^2, \tag{A.19b}$$

$$E_{h2}^{n+(1/2)} = \frac{\rho}{2}\left\|\frac{\mathbf{u}_h^{n+1}-\mathbf{u}_h^n}{\Delta t}\right\|_0^2 - \frac{\Delta t^2}{4}\sum_{k=1}^{N_f}\left(\frac{\mathbf{s}_{hk}^{n+1}-\mathbf{s}_{hk}^n}{\Delta t}, \mathbf{D}_h\left(\frac{\mathbf{u}_h^{n+1}-\mathbf{u}_h^n}{\Delta t}\right)\right)_{1/2} - \frac{\Delta t^2}{8}\left(H_0 + \sum_{k=1}^{N_f}\frac{H_{0k}}{1-p_k}\right)\left\|\mathbf{D}_h\left(\frac{\mathbf{u}_h^{n+1}-\mathbf{u}_h^n}{\Delta t}\right)\right\|_{1/2}^2 - \sum_{k=1}^{N_f}\frac{\Delta t^2(1-p_k^2)}{16H_{0k}p_k}\left\|\frac{\mathbf{s}_{hk}^{n+1}-\mathbf{s}_{hk}^n}{\Delta t}\right\|_{1/2}^2. \tag{A.19c}$$

Let us note that Eq. (A.19b) on $E_{h1}^{n+(1/2)}$ may be rewritten using the Z-transform $H(z)$ of Filter (7) as

$$E_{h1}^{n+(1/2)} = \frac{H(1)}{2}\left\|\mathbf{D}_h\left(\frac{\mathbf{u}_h^{n+1}+\mathbf{u}_h^n}{2}\right)\right\|_{1/2}^2 - \sum_{k=1}^{N_f}\frac{1-p_k^2}{4H_{0k}p_k}\left\|\frac{\mathbf{s}_{hk}^{n+1}+\mathbf{s}_{hk}^n}{2}\right\|_{1/2}^2.$$

Then, sufficient conditions in order to ensure the positivity of $E_{h1}^{n+(1/2)}$ are

$$H(1) \geq 0 \quad \text{and} \quad H_{0k}p_k \leq 0 \quad k = \{1, \ldots, N_f\}, \tag{A.20}$$

which also ensure the positivity of the dissipation D_h^n (A.18a).

In order to study $E_{h2}^{n+(1/2)}$, assuming that H_{0k} and p_k satisfy the previous condition, we start by expanding the following inequality:

$$\left\|\sqrt{-\frac{(1-p_k^2)}{2H_{0k}p_k}}\left(\frac{\mathbf{s}_{hk}^{n+1}-\mathbf{s}_{hk}^n}{\Delta t}\right) - \sqrt{-\frac{2H_{0k}p_k}{1-p_k^2}}\mathbf{D}_h\left(\frac{\mathbf{u}_h^{n+1}-\mathbf{u}_h^n}{\Delta t}\right)\right\|_{1/2}^2 \geq 0,$$

which yields when being multiplied by $\Delta t^2/8$:

$$-\frac{\Delta t^2}{16}\frac{1-p_k^2}{H_{0k}p_k}\left\|\frac{\mathbf{s}_{hk}^{n+1}-\mathbf{s}_{hk}^n}{\Delta t}\right\|_{1/2}^2 - \frac{\Delta t^2}{4}\left(\frac{\mathbf{s}_{hk}^{n+1}-\mathbf{s}_{hk}^n}{\Delta t}, \mathbf{D}_h\left(\frac{\mathbf{u}_h^{n+1}-\mathbf{u}_h^n}{\Delta t}\right)\right)_{1/2} \geq \frac{\Delta t^2}{4}\frac{H_{0k}p_k}{1-p_k^2}\left\|\mathbf{D}_h\left(\frac{\mathbf{u}_h^{n+1}-\mathbf{u}_h^n}{\Delta t}\right)\right\|_{1/2}^2. \tag{A.21}$$

Then, substituting Eq. (A.21) in Eq. (A.19c) gives a first lower bound for $E_{h2}^{n+(1/2)}$ as

$$E_{h2}^{n+(1/2)} \geq \frac{\rho}{2}\left\|\frac{\mathbf{u}_h^{n+1}-\mathbf{u}_h^n}{\Delta t}\right\|_0^2 - \frac{\Delta t^2}{8}\left(H_0 + \sum_{k=1}^{N_f}\frac{H_{0k}}{1+p_k}\right)\left\|\mathbf{D}_h\left(\frac{\mathbf{u}_h^{n+1}-\mathbf{u}_h^n}{\Delta t}\right)\right\|_{1/2}^2. \tag{A.22}$$

Furthermore, let us note the following result for all $\mathbf{v}_h \in L^2(\Omega_{h,0})$:

$$\|\mathbf{D}_h\mathbf{v}_h\|_{1/2}^2 = \frac{1}{h}\sum_{j=0}^{N_x-1}\left(\mathbf{v}_{hj+1}^2 + \mathbf{v}_{hj}^2 - 2\mathbf{v}_{hj+1}\mathbf{v}_{hj}\right) \le \frac{2}{h}\sum_{j=0}^{N_x-1}\left(\mathbf{v}_{hj+1}^2 + \mathbf{v}_{hj}^2\right) \le \frac{4}{h^2}\|\mathbf{v}_h\|_0^2, \tag{A.23}$$

which gives

$$\left\|\mathbf{D}_h\left(\frac{\mathbf{u}_h^{n+1}-\mathbf{u}_h^n}{\Delta t}\right)\right\|_{1/2}^2 \le \frac{4}{h^2}\left\|\frac{\mathbf{u}_h^{n+1}-\mathbf{u}_h^n}{\Delta t}\right\|_0^2. \tag{A.24}$$

Using this last result allows us to derive a new lower bound on $E_{h2}^{n+(1/2)}$ as

$$E_{h2}^{n+(1/2)} \ge \frac{1}{2}\left[\rho - \frac{\Delta t^2}{h^2}\left(H_0 + \sum_{k=1}^{N_f}\frac{H_{0k}}{1+p_k}\right)\right]\left\|\frac{\mathbf{u}_h^{n+1}-\mathbf{u}_h^n}{\Delta t}\right\|_0^2. \tag{A.25}$$

Finally, a sufficient condition that ensure positivity of $E_{h2}^{n+(1/2)}$, involving the discretization parameters h and Δt is

$$\rho - \frac{\Delta t^2}{h^2}\left(H_0 + \sum_{k=1}^{N_f}\frac{H_{0k}}{1+p_k}\right) \ge 0. \tag{A.26}$$

We recognize here a classic CFL condition, which may be rewritten in a more compact way involving transfer function $H(z)$ as

$$\Delta t \le h\sqrt{\frac{\rho}{H(-1)}}. \tag{A.27}$$

Appendix B. Reference modal solution

This section describes the modal analysis performed in order to obtain the reference solution used for validating our numerical results in Section 5.3. To do so, we start again from the equation setting of our model problem and look for an analytical solution in separated variables form:

$$u(x,t) = X(x)T(t). \tag{B.1}$$

First of all, we apply the partial time-domain Fourier transform to Eq. (1), where the volumetric force density has been chosen as $f(x,t) = F(t)\delta(x-L) = F(t)\delta_L(x)$ as in Section 5. Using the linear and local property of the constitutive law $\mathcal{E}$ yields

$$-\rho\omega^2\hat{u}(x,\omega) - E^*(\omega)\frac{\partial^2\hat{u}(x,\omega)}{\partial x^2} = \delta_L(x)\hat{F}(\omega), \tag{B.2}$$

where $E^*(\omega)$ is the frequency-domain response of operator $\mathcal{E}$, $\hat{F}(\omega)$ is the Fourier transform of $F(t)$ and $\hat{u}(x,\omega)$ writes $\hat{u}(x,\omega) = X(x)\hat{T}(\omega)$.

Next, substituting the separated form (B.1) in the homogeneous counterpart of Eq. (B.2) gives the classical eigenvalue problem in terms of the space function X:

$$\frac{\partial^2 X(x)}{\partial x^2} + k^2 X(x) = 0.$$

Solving the previous problem together with the choice of clamped–free boundary conditions given in Eq. (2.1) allows us to express the following orthonormalized family of functions $\{X_n\}_{n\in\mathbb{N}^*}$ which is the modal basis of Problem (1):

$$X_n(x) = \sqrt{\frac{2}{L}}\sin(k_n x) \quad \text{with} \quad k_n = \left(n-\frac{1}{2}\right)\frac{\pi}{L} \quad (n\in\mathbb{N}^*), \tag{B.3}$$

where the usual L^2 norm $\|X_n\|$ has been used for normalization:

$$\|X_n\| = \left[\int_0^L X_n(x)^2\,dx\right]^{1/2}.$$

Let us recall the fundamental properties of family $\{X_n\}_{n\in\mathbb{N}^*}$:

$$(X_n, X_m) = \delta_{n,m} \quad \text{and} \quad \frac{\partial^2 X_n(x)}{\partial x^2} = -k_n^2 X_n(x),$$

where (X_n, X_m) denotes the usual L^2 scalar product:

$$(X_n, X_m) = \int_0^L X_n(x)X_m(x)\,dx.$$

We now express the solution $\hat{u}(x,\omega)$ of the space-frequency-domain problem on Basis (B.3):

$$\hat{u}(x,\omega) = \sum_{n=1}^{\infty} X_n(x)\hat{T}_n(\omega), \tag{B.4}$$

and substitute this expression into Eq. (B.2):

$$\sum_{n=1}^{\infty} \left(-\rho\omega^2 + k_n^2 E^*(\omega)\right) X_n(x)\hat{T}_n(\omega) = \delta_L(x)\hat{F}(\omega).$$

Next, the orthogonality property allows us to express $\hat{T}_n(\omega)$ as

$$\hat{T}_n(\omega) = \frac{\hat{F}(\omega)}{-\rho\omega^2 + k_n^2 E^*(\omega)} \frac{(\delta_L, X_n)}{\|X_n\|^2}.$$

Noting that $\|X_n\|^2 = 1$ and $(\delta_L, X_n) = X_n(L)$, the frequency-domain analytical solution of model Problem (1) is given as follows:

$$\hat{u}(x,\omega) = \sum_{n=1}^{\infty} \frac{\hat{F}(\omega)}{-\rho\omega^2 + k_n^2 E^*(\omega)} X_n(L)X_n(x). \tag{B.5}$$

Finally, in order to compute the reference modal solution used to compare the numerical results of Section 5.3, we set $E^*(\omega) = H^c(\omega)$ and truncate the infinite sum of Eq. (B.5) to 212 modes, which corresponds to all the modes up to 180 kHz.

References

[1] S. Crandall, The role of damping in vibration theory, J. Sound Vib. 11 (1) (1970) 3–18, http://dx.doi.org/10.1016/S0022-460X(70)80105-5.
[2] L. Gaul, The influence of damping on waves and vibrations, Mech. Syst. Signal Process. 13 (1) (1999) 1–30, http://dx.doi.org/10.1006/mssp.1997.0185.
[3] M.D. Rao, Recent applications of viscoelastic damping for noise control in automobiles and commercial airplanes, J. Sound Vib. 262 (3) (2003) 457–474, http://dx.doi.org/10.1016/S0022-460X(03)00106-8.
[4] T.X. Wu, D.J. Thompson, On the impact noise generation due to a wheel passing over rail joints, J. Sound Vib. 267 (3) (2003) 485–496, http://dx.doi.org/10.1016/S0022-460X(03)00709-0.
[5] M. Vorländer, Auralization of spaces, Phys. Today 62 (6) (2009) 35–40, http://dx.doi.org/10.1063/1.3156831.
[6] S. Bilbao, Numerical Sound Synthesis, 1st ed., Wiley, 2009 (ISBN 9780470510469).
[7] A. Chaigne, V. Doutaut, Numerical simulations of xylophones. I. Time-domain modeling of the vibrating bars, J. Acous. Soc. Am. 101 (1) (1997) 539–557, http://dx.doi.org/10.1121/1.418117.
[8] E. Bécache, A. Chaigne, G. Derveaux, P. Joly, Numerical simulation of a guitar, Comput. Struct. 83 (2–3) (2005) 107–126, http://dx.doi.org/10.1016/j.compstruc.2004.04.018.
[9] J. Chabassier, A. Chaigne, P. Joly, Modeling and simulation of a grand piano, J. Acoust. Soc. Am. 134 (1) (2013) 648–665, http://dx.doi.org/10.1121/1.4809649.
[10] S. McAdams, V. Roussarie, A. Chaigne, B.L. Giordano, The psychomechanics of simulated sound sources: material properties of impacted thin plates, J. Acoust. Soc. Am. 128 (3) (2010) 1401–1413, http://dx.doi.org/10.1121/1.3466867.
[11] J. Soovere, M. Drake, Aerospace Structures Technology Damping Design Guide, Volume III – Damping Material Data, AFWAL-TR-84-3089, Air Force Wright Aeronautical Laboratories, 1985.
[12] T. Pritz, Frequency power law of material damping, Appl. Acoust. 65 (11) (2004) 1027–1036, http://dx.doi.org/10.1016/j.apacoust.2004.06.001.
[13] R.M. Christensen, Theory of Viscoelasticity, Civil, Mechanical and Other Engineering Series, Dover, Mineola, NY, USA 2003 (ISBN 9780486428802).
[14] D.F. Golla, P.C. Hughes, Dynamics of viscoelastic structures—a time-domain, finite element formulation, J. Appl. Mech. 52 (4) (1985) 897–906, http://dx.doi.org/10.1115/1.3169166.
[15] D.J. McTavish, P.C. Hughes, Modeling of linear viscoelastic space structures, J. Vib. Acoust. 115 (1) (1993) 103–110, http://dx.doi.org/10.1115/1.2930302.
[16] G. Lesieutre, E. Bianchini, Time domain modeling of linear viscoelasticity using anelastic displacement fields, J. Vib. Acoust. 117 (1995) 424–430.
[17] A. Chaigne, C. Lambourg, Time-domain simulation of damped impacted plates. I. Theory and experiments, J. Acoust. Soc. Am. 109 (4) (2001) 1422–1432 , http://dx.doi.org/10.1121/1.1354200.
[18] E. Bécache, A. Ezziani, P. Joly, A mixed finite element approach for viscoelastic wave propagation, Comput. Geosci. 8 (3) (2005) 255–299, http://dx.doi.org/10.1007/s10596-005-3772-8.
[19] R.L. Bagley, P.J. Torvik, Fractional calculus—a different approach to the analysis of viscoelastically damped structures, AIAA J. 21 (5) (1983) 741–748, http://dx.doi.org/10.2514/3.8142.
[20] A. Lion, On the thermodynamics of fractional damping elements, Contin. Mech. Thermodyn. 9 (2) (1997) 83–96, http://dx.doi.org/10.1007/s001610050057.
[21] J.-F. Deü, D. Matignon, Simulation of fractionally damped mechanical systems by means of a Newmark-diffusive scheme, Comput. Math. Appl. 59 (5) (2010) 1745–1753, http://dx.doi.org/10.1016/j.camwa.2009.08.067.
[22] P. Collet, G. Gary, B. Lundberg, Noise-corrected estimation of complex modulus in accord with causality and thermodynamics: application to an impact test, J. Appl. Mech. 80 (1) (2013) 1018–1024, http://dx.doi.org/10.1115/1.4007081.
[23] J.O. Smith, Introduction to Digital Filters with Audio Applications, Music Signal Processing Series, W3K Publishing, 2007 (ISBN 9780974560717).
[24] A.V. Oppenheim, R.W. Schafer, Discrete-Time Signal Processing, Prentice Hall, 3rd ed., Upper Saddle River, New Jersey, USA 2009 (ISBN 9780132146357).
[25] F. Renaud, J.-L. Dion, G. Chevallier, I. Tawfiq, R. Lemaire, A new identification method of viscoelastic behavior: application to the generalized Maxwell model, Mech. Syst. Signal Process. 25 (3) (2011) 991–1010, http://dx.doi.org/10.1016/j.ymssp.2010.09.002.
[26] J. Bonnans, J. Gilbert, C. Lemaréchal, C. Sagastizábal, Numerical Optimization, Theoretical and Practical Aspects, Springer-Verlag, 2nd ed., Berlin, Heidelberg, Germany, 2006 (ISBN 9783540354475).
[27] M. Mossberg, L. Hillström, T. Söderström, Non-parametric identification of viscoelastic materials from wave propagation experiments, Automatica 37 (4) (2001) 511–521, http://dx.doi.org/10.1016/S0005-1098(00)00188-6.
[28] R. Pintelon, P. Guillaume, S. Vanlanduit, K. De Belder, Y. Rolain, Identification of Young's modulus from broadband modal analysis experiments, Mech. Syst. Signal Process. 18 (4) (2004) 699–726, http://dx.doi.org/10.1016/S0888-3270(03)00045-1.
[29] J. Robertsson, J. Blanch, W. Symes, Viscoelastic finite-difference modeling, Geophysics 59 (9) (1994) 1444–1456, http://dx.doi.org/10.1190/1.1443701.